19. Inoue M, Iwasaki M, Otani T, Sasazuki S, Tsugane S. Public awareness of risk factors for cancer among the Japanese general population: a population-based survey. BMC Public Health. 2006;6:2.
20. Sato T, Iwaki M, Shimogaito N, Wu X, Yamagishi S, Takeuchi M. TAGE (toxic AGEs) theory in diabetic complications. Curr Mol Med. 2006;6:351–8.
21. Yao D, Brownlee M. Hyperglycemia-induced reactive oxygen species increase expression of the receptor for advanced glycation end products (RAGE) and RAGE ligands. Diabetes. 2010;59:249–55.
22. Nishikawa T, Edelstein D, Du XL, Yamagishi S, Matsumura T, Kaneda Y, et al. Normalizing mitochondrial superoxide production blocks three pathways of hyperglycaemic damage. Nature. 2000;404:787–90.
23. Schurman L, McCarthy AD, Sedlinsky C, Gangoiti MV, Arnol V, Bruzzone L, et al. Metformin reverts deleterious effects of advanced glycation end-products (AGEs) on osteoblastic cells. Exp Clin Endocrinol Diabetes. 2008;116:333–40.
24. Bellin C, de Wiza DH, Wiernsperger NF, Rosen P. Generation of reactive oxygen species by endothelial and smooth muscle cells: influence of hyperglycemia and metformin. Horm Metab Res. 2006;38:732–9.
25. Sebekova K, Schinzel R, Munch G, Krivosikova Z, Dzurik R, Heidland A. Advanced glycation end-product levels in subtotally nephrectomized rats: beneficial effects of angiotensin II receptor 1 antagonist losartan. Miner Electrolyte Metab. 1999;25:380–3.
26. Singh J, Hamid R, Reddy BS. Dietary fish oil inhibits the expression of farnesyl protein transferase and colon tumor development in rodents. Carcinogenesis. 1998;19:985–9.
27. Rao CV, Simi B, Wynn TT, Garr K, Reddy BS. Modulating effect of amount and types of dietary fat on colonic mucosal phospholipase A2, phosphatidylinositol-specific phospholipase C activities, and cyclooxygenase metabolite formation during different stages of colon tumor promotion in male F344 rats. Cancer Res. 1996;56:532–7.
28. Zhou S, Wang G, Chen B, Wang P. Effect of dietary fatty acids on tumorigenesis of colon cancer induced by methyl nitrosourea in rats. J Environ Pathol Toxicol Oncol. 2000;19:81–6.
29. Simopoulos AP. Evolutionary aspects of diet, the omega-6/omega-3 ratio and genetic variation: nutritional implications for chronic diseases. Biomed Pharmacother. 2006;60:502–7.
30. Simopoulos AP. Essential fatty acids in health and chronic disease. Am J Clin Nutr. 1999;70:560S–9S.
31. McLellan EA, Medline A, Bird RP. Sequential analyses of the growth and morphological characteristics of aberrant crypt foci: putative preneoplastic lesions. Cancer Res. 1991;51:5270–4.
32. Pugliese G, Pricci F, Leto G, Amadio L, Iacobini C, Romeo G, et al. The diabetic milieu modulates the advanced glycation end product-receptor complex in the mesangium by inducing or upregulating galectin-3 expression. Diabetes. 2000;49:1249–57.
33. Shimoda H, Nakamura S, Morioka M, Tanaka J, Matsuda H, Yoshikawa M. Effect of cinnamoyl and flavonol glucosides derived from cherry blossom flowers on the production of advanced glycation end products (AGEs) and AGE-induced fibroblast apoptosis. Phytother Res. 2011.
34. De Bellis D, Horowitz MI. In vitro studies of histone glycation. Biochim Biophys Acta. 1987;926:365–8.
35. Bull NL. Dietary habits, food consumption, and nutrient intake during adolescence. J Adolesc Health. 1992;13:384–8.
36. Campos FG, Logullo Waitzberg AG, Kiss DR, Waitzberg DL, Habr-Gama A, Gama-Rodrigues J. Diet and colorectal cancer: current evidence for etiology and prevention. Nutr Hosp. 2005;20:18–25.
37. Stern DM, Yan SD, Yan SF, Schmidt AM. Receptor for advanced glycation endproducts (RAGE) and the complications of diabetes. Ageing Res Rev. 2002;1:1–15.
38. Li J, Schmidt AM. Characterization and functional analysis of the promoter of RAGE, the receptor for advanced glycation end products. J Biol Chem. 1997;272:16498–506.
39. Li J, Qu X, Schmidt AM. Sp1-binding elements in the promoter of RAGE are essential for amphoterin-mediated gene expression in cultured neuroblastoma cells. J Biol Chem. 1998;273:30870–8.
40. Huttunen HJ, Rauvala H. Amphoterin as an extracellular regulator of cell motility: from discovery to disease. J Intern Med. 2004;255:351–66.
41. Yan SD, Chen X, Fu J, Chen M, Zhu H, Roher A, et al. RAGE and amyloid-beta peptide neurotoxicity in Alzheimer's disease. Nature. 1996;382:685–91.
42. Ohmori H, Luo Y, Fujii K, Sasahira T, Shimomoto T, Denda A, et al. Dietary linoleic acid and glucose enhances azoxymethane-induced colon cancer and the metastasis through the expression of high mobility group box 1. Pathobiology. 2010;77:210–7.
43. Lee CI, Guh JY, Chen HC, Hung WC, Yang YL, Chuang LY. Advanced glycation end-product-induced mitogenesis and collagen production are dependent on angiotensin II and connective tissue growth factor in NRK-49F cells. J Cell Biochem. 2005;95:281–92.
44. Leiter LA, Lewanczuk RZ. Of the renin-angiotensin system and reactive oxygen species type 2 diabetes and angiotensin II inhibition. Am J Hypertens. 2005;18:121–8.
45. Yamamoto K, Kitayama W, Denda A, Morisaki A, Kuniyasu H, Kirita T. Inhibitory effects of selective cyclooxygenase-2 inhibitors, nimesulide and etodolac, on the development of squamous cell dysplasias and carcinomas of the tongue in rats initiated with 4-nitroquinoline 1-oxide. Cancer Lett. 2003;199:121–9.
46. Ge QM, Dong Y, Su Q. Effects of glucose and advanced glycation end products on oxidative stress in MIN6 cells. Cell Mol Biol (Noisy-le-grand). 2010;56 Suppl:OL1231–8.
47. Reddy VP, Beyaz A. Inhibitors of the Maillard reaction and AGE breakers as therapeutics for multiple diseases. Drug Discov Today. 2006;11:646–54.
48. Rahbar S. Novel inhibitors of glycation and AGE formation. Cell Biochem Biophys. 2007;48:147–57.

British Journal of Cancer (2012), 1–7

www.bjcancer.com

Full Paper

Downregulation of miR-126 induces angiogenesis and lymphangiogenesis, and targets VEGF-A in oral cancer

T Sasahira[1], M Kurihara[1,2], UK Bhawal[1,3], N Ueda[2], T Shimomoto[1], K Yamamoto[2], T Kirita[2] and H Kuniyasu*[,1]

[1]Department of Molecular Pathology, Nara Medical University School of Medicine, 840 Shijo-cho, Kashihara, Nara 634-8521, Japan; [2]Department of Oral and Maxillofacial Surgery, Nara Medical University School of Medicine, 840 Shijo-cho, Kashihara, Nara 634-8521, Japan; [3]Department of Biochemistry and Molecular Biology, Nihon University School of Dentistry at Matsudo, Matsudo, Japan

BACKGROUND: MicroRNA (miRNA)-126 (*miR-126*) is an endothelial-specific miRNA located within intron 7 of epidermal growth factor-like domain 7 (*EGFL7*). However, the role of *miR-126* in cancer is controversial.

METHODS: We examined the function of *miR-126* in oral squamous cell carcinoma (OSCC) cells. Furthermore, a series of 118 cases with OSCC were evaluated for the expression levels of miR-126.

RESULTS: MicroRNA-126 (*miR-126*) was associated with cell growth and regulation of vascular endothelial growth factor-A activity, and demethylation treatment increased expression levels of *miR-126* and *EGFL7* in OSCC cells. A significant association was found between *miR-126* expression and tumour progression, nodal metastasis, vessel density, or poor prognosis in OSCC cases. In the multivariate analysis, decreased *miR-126* expression was strongly correlated with disease-free survival.

CONCLUSION: The present results suggest that *miR-126* might be a useful diagnostic and therapeutic target in OSCC.

British Journal of Cancer (2012) **0,** 000–000. doi:10.1038/bjc.2012.330 www.bjcancer.com

Keywords: miR-126; oral squamous cell carcinoma; angiogenesis; lymphangiogenesis; VEGF-A

Head and neck cancer, including oral squamous cell carcinoma (OSCC), is the sixth most common cancer worldwide (Argiris *et al*, 2008). The incidence of OSCC is estimated at 263 900 cases and 128 000 deaths annually (Jemal *et al*, 2011), and an estimated 7850 patients die from this disease in the United States (Siegel *et al*, 2012). Oral squamous cell carcinoma has a high potential for local invasion and lymph node metastasis, and overall 5-year survival rates have not significantly improved during the past three decades (Dos Reis *et al*, 2008). The 5-year survival rate in OSCC is less than 50% (Marsh *et al*, 2011). Although more than 80% of early-stage OSCCs can be cured by treatment, approximately 70% of advanced-stage patients cannot be cured (Mydlarz *et al*, 2010). Therefore, early detection and clarification of detailed molecular mechanism of OSCC is a problem of the urgent business.

MicroRNAs (miRNAs) are non-coding small RNAs, approximately 18–25 nucleotides in length (Bartel, 2009; Martello *et al*, 2010), which function as suppressors of gene expression by binding to the 3′-untranslated region (UTR) of target mRNAs (Calin and Croce, 2006; Liu *et al*, 2010; Martello et al., 2010). MicroRNA-126 (*miR-126*) is located within intron 7 of epidermal growth factor-like domain 7 (*EGFL7*) and is highly expressed in vascular endothelial cells (Fish *et al*, 2008; Wang *et al*, 2008a). In tumour cells, *miR-126* acts as a tumour suppressor gene in many malignant tumour cells (Wang *et al*, 2008b; Liu *et al*, 2009; Saito *et al*, 2009; Feng *et al*, 2010; Miko *et al*, 2011; Zhu *et al*, 2011). MicroRNA-126 (*miR-126*) is significantly expressed lower in carcinoma as compared with adenoma and useful diagnostic marker after thyroid fine-needle aspiration biopsy (Kitano *et al*, 2011). MicroRNA-126 (*miR-126*) is also strongly downregulated in pancreatic cancer, with an associated elevation in *K-Ras* (Slaby *et al*, 2012), and lower expression of *miR-126* is significantly correlated with short survival in non-small cell lung carcinoma (NSCLC) and renal cell carcinoma (Donnem *et al*, 2012; Jiao *et al*, 2012). Further, Yu *et al* (2009) have reported downregulation of *miR-126* to promote oral carcinogenesis in Syrian hamster. Saito *et al* (2009) showed that *miR-126* and *EGFL7*, which is the host gene for *miR-126*, are downregulated by DNA hypermethylation, and *miR-126* and *EGFL7* expression are restored after treatment with 5-aza-2′-deoxycytidine (5-Aza-dc) in urologic cancer. Silencing of *miR-126* by the DNA methylation of *EGFL7* was also reported in NSCLC (Watanabe *et al*, 2012). However, several reports have described an oncogenic role for *miR-126*, such as the inhibition of apoptosis in acute myeloid leukaemia and the promotion of gastric carcinogenesis (Otsubo *et al*, 2011). In addition, higher expression of *miR-126* was shown to be a poor prognostic factor in NSCLC (Donnem *et al*, 2011) and promote metastasis in prostate cancer (Watahiki *et al*, 2011). Meister and Schmidt (2010) recently reported that higher expression of *miR-126* accelerates cancer progression by activation of mitogen-activated protein kinase and Akt, whereas miR-126 suppresses tumour proliferation and invasion because of decreased Crk expression. These contradictory findings suggest that *miR-126* has several functions specific to each type of malignancy.

Angiogenesis has a pivotal role in prenatal development, wound healing, chronic inflammation, tumour progression, and metastasis (Carmeliet, 2005; Sasahira *et al*, 2007a), and lymphangiogenesis promotes lymph node metastasis in cancer cells (Adams and Alitalo, 2007; Sasahira *et al*, 2010). Vascular endothelial growth factor (*VEGF*)-*A* and *VEGF-C/D* are one of the representative factors of angiogenesis and/or lymphangiogenesis (Adams and

*Correspondence: Dr H Kuniyasu; E-mail: cooninh@zb4.so-net.ne.jp
Received 16 April 2012; revised 27 June 2012; accepted 3 July 2012

Alitalo, 2007), and we have also previously reported that the VEGF family induce angiogenesis and/or lymphangiogenesis in OSCC (Sasahira *et al*, 2007a,b, 2008, 2010). However, several reports have revealed that VEGF-A is not related with angiogenesis and VEGF-C/D are not associated with nodal metastasis in cancer (Santos *et al*, 2003; Currie *et al*, 2004; Nomiya *et al*, 2006; Miyahara *et al*, 2007; Donnem *et al*, 2009). It has also been reported that vessel numbers in nodal metastasis cases are lower than cases without metastasis (Moriyama *et al*, 1997). Thus, the role of tumour angiogenesis and lymphangiogenesis are still controversial.

Recently, it was reported that *VEGF-A* is a target gene of *miR-126* and downregulation of *miR-126* increases *VEGF-A* activity in lung (Liu *et al*, 2009; Zhu *et al*, 2012) and breast cancer (Zhu *et al*, 2011). However, other reports indicated that *miR-126* is an inducer of angiogenesis by enhancing the proangiogenic activity of *VEGF-A* (Fish *et al*, 2008; Wang *et al*, 2008a). Thus, *miR-126* may function differently in tumour cells and stromal cells. In this study, we examined the angiogenic role of *miR-126* and confirmed the relationship between the expression of *miR-126* and lymphangiogenesis in OSCC.

MATERIALS AND METHODS

Cell culture

Human OSCC cell lines, HSC3 and HSC4 cells, were obtained from the Health Science Research Resources Bank and maintained in Dulbbeco's modified Eagle's medium (DMEM; Wako Pure Chemical industries, Ltd, Osaka, Japan) supplemented with 10% fetal bovine serum (Sigma Chemical, St Louis, MO, USA) under the conditions of 5% CO_2 in air at 37 °C. The HSC3 cells have high metastatic potential and HSC4 cells have low metastatic ability (Sasahira *et al*, 2010).

RNA isolation and quantitative reverse-transcription PCR

Total RNA and small RNA were extracted using RNeasy Mini Kit (Qiagen, Valencia, CA, USA) or *mir*Vana miRNA Isolation Kit (Ambion, Austin, TX, USA), and total RNA (1 μg) and small RNA (10 ng) were synthesised with the ReverTra Ace qRT Kit (Toyobo, Osaka, Japan) or TaqMan MicroRNA RT Kit (Applied Biosystems, Foster City, CA, USA), respectively. Quantitative reverse-transcription PCR (qRT–PCR) were performed on StepOne Plus Real-Time PCR Systems (Applied Biosystems) using EXPRESS qPCR Supermixes (Invitrogen, Carlsbad, CA, USA) and analyse the relative standard curve quantification method. The PCR condition was according to the manufacturer's instructions and *18S* (eukaryotic 18S rRNA) expression level was amplified for internal control. TaqMan MicroRNA assays of hsa-*miR-126* and TaqMan Gene Expression Assays of *VEGF-A*, *VEGF-C*, *VEGF-D*, *EGFL7*, and *18S* were purchased from Applied Biosystems. All PCRs were performed in triplicates.

Methylation-specific PCR

For the bisulfite modification of DNA, 2 μg of genomic DNA extracted using the QIAamp DNA Mini kit (Qiagen) was treated with the Epitect Bisulfite kit (Qiagen) according to the provider's manual. For analysis of DNA methylation of *EGFL7*, we carried out methylation-specific PCR (MSP) using an Epitect MSP kit (Qiagen). The PCR products were separated by 6% non-denaturing polyacrylamide gels, stained with ethidium bromide (Sigma Chemical), and visualised under UV light.

The sequences of the primers methylated or unmethylated of *EGFL7* are as follows (Saito *et al*, 2009): 5′-GTG GTG GTG GTG TGT GTG TGT TT-3′ and 5′-CTC AAC CCA ACC CAA ACA ACA ACC A-3′ for unmethylated *EGFL7*; 5′-GCG GCG CGT GCG CGT TT-3′ and 5′-CCA ACC CGA ACG ACG ACC G-3′ for methylated *EGFL7*.

DNA demethylation treatment

Previous results raise the possibility that *miR-126* expression is regulated by DNA methylation (Saito *et al*, 2009). Therefore, we performed the demethylation treatment in OSCC cells. Each cell was seeded at a density of 1×10^6 cells ml^{-1}. After 24 h, cells were treated with 1 μM 5-Aza-dc (Sigma Chemical) for 4 days. Treatment with 300 nM trichostatin A (TSA; Sigma Chemical) was also performed for 24 h. Cells then were harvested for miRNA extractions.

Transient transfection

Pre-*miR-126* precursor, anti-*miR126* inhibitor, pre-miR negative control 1, and anti-miR negative control 1 were purchased from Ambion. Pre-miR (10 nM) and anti-miR (30 nM) were transfected with Lipofectamine 2000 (Invitrogen) according to the provider's recommendations.

Cell growth assay

The cells were seeded at density of 2000 cells per well of 96-well tissue culture plates and incubated for 48 h at 37 °C. Cell growth was assessed by MTT assay using the incorporation of 3-(4,5-dimethylthiazol-2-yl)-2,5-diphenyltetrazolium bromide (Sigma Chemical). The experiments were performed in triplicates.

In vitro invasion assay

A modified Boyden chamber assay was performed using the BD BioCoat Cell Culture Inserts glued to type IV collagen (Becton-Dickinson, Bedford, MA, USA) as described previously. Cells were suspended in 500 μl of DMEM and placed 4 in the insert. After 48 h incubation at 37 °C, the filters were stained with haematoxylin. The stained cells were counted in whole inserts at × 100 magnification. Each experiment was repeated at least three times.

Apoptosis assay

Apoptotic cells were detected by the terminal deoxynucleotidyl trsnsferase (TdT)-mediated dUTP-biotin nick and labelling (TUNEL) assay using the *In Situ* Cell Death Detection Kit, POD (Roche Diagnostics, Indianapolis, IN, USA). We also confirmed the activation of caspase-3 was detected using CaspACE Assay system, Colorimetric (Promega, Madison, WI, USA) according to the manufacturer's protocol. The experiments were performed in triplicates.

Oral squamous cell carcinoma samples

One-hundred and eighteen patients (68 men, 50 women; 46–91 years of age, mean: 67.4 years) of primary OSCCs, who were treated at Nara Medical University Hospital, Kashihara, Japan, from February 2000 to October 2008, were randomly selected. Tumours were staged according to the UICC TNM classification system, 7th edition, and histopathological grading was in accordance with the World Health Organization criteria. None of the patients was treated before surgery and sample preparation. Medical records and prognostic follow-up data were obtained from the patient database maintained by the hospital. The median follow-up period was 3.4 years (range 0.5–5.9). For strict privacy protection, identifying information for all samples was removed before analysis. This procedure was in accordance with the Ethical Guidelines for Human Genome/Gene Research of the Japanese Government. To determine the relation between *miR-126*

expression and clinicopathological characteristics, we divided into two groups according to expression levels those with values higher the mean value for the entire group and those with than the group mean value. Ten samples of normal oral mucosa (six man, four woman; 20–47 years of age, mean: 37.9 years) were used as control.

Laser-capture microdissection

As previous reports suggested that functions of *miR-126* are different in cancer cells and stromal cells (Fish *et al*, 2008; Wang *et al*, 2008a; Liu *et al*, 2009; Zhu *et al*, 2011), we performed the laser-capture microdissection (LCM) to selectively extract small RNA from OSCC cells. Tissue sections (7 μm) were prepared from each paraffin blocks and stained using haematoxylin and eosin. Slides were transferred for microdissection using a Pix Cell II laser capture microscope (Arcturus, Mountain View, CA, USA) according to the manufacturer's instructions. Approximately 5000 tumour cells were microdissected from each tissue. MicroRNA was extracted using the *mir*Vana miRNA Isolation Kit (Ambion).

Immunohistochemistry

Immunohistochemical analysis was performed with the EnVision+ DualLink (DAKO, Carpinteria, CA, USA) system and antigen retrieval was performed with microwaving in citrate buffer at 95 °C for 45 min. After endogeneous peroxidase block by 3% H_2O_2-methanol, anti-CD34 antibody (a marker for vascular endothelial cells; DAKO) and anti-LYVE-1 antibody (a marker for lymphovascular endothelial cells; Abcam, Tokyo, Japan) were used for primary antibody for 2 h and incubated with the secondary antibody for 30 min at room temperature. The specimens were colour-developed with diaminobenzidine solution (DAKO) and specimens were counterstained with Mayer's haematoxylin (Sigma Chemical). The MVD and LVD were measured on anti-CD34 and anti-LYVE-1 antibody immunopositive specimens, respectively. To quantify MVD or LVD, five maximum vessel-density fields were selected from around of the tumour cells (the 'hot spot') and examined under a 200-fold magnification by a microscope and averaged. We divided the tissue samples into two groups according to MVD levels: those with values higher than the mean value for the entire group, and those with lower values than the group mean value. The same was applied based on the LVD values.

Statistical analysis

The correlation of variables was performed by Fischer's exact test, one-factor ANOVA test, and Mann–Whitney *U*-test. Disease-free survival analysis was calculated using the Kaplan–Meier method, and differences between groups were tested by means of a log lank test. Univariate analysis for disease-free survival was calculated by log lank test. For multivariate analysis, Cox proportional hazards model was used (described as risk ratio with 95% confidence intervals, together with the *P*-value). All statistical analysis was carried out with JMP8 (SAS Institute, Cary, NC, USA). *P*-values less than 0.05 were regarded as statistically significant.

RESULTS

Expression of miR-126 and EGFL7 in OSCC cells

The expressions of *miR-126* and *EGFL7*, which is the host gene of *miR-126*, were examined by qRT–PCR in the HSC3 and HSC4 cells. The expression levels of *miR-126* and *EGFL7* in the HSC3 cells with high metastatic potential were approximately 10 times lower than HSC4 cells with low metastatic potential (Figures 1A and B). Examination of the methylation status of *EGFL7* by MSP showed the presence of a methylated *EGFL7* band in the HSC3 cells that

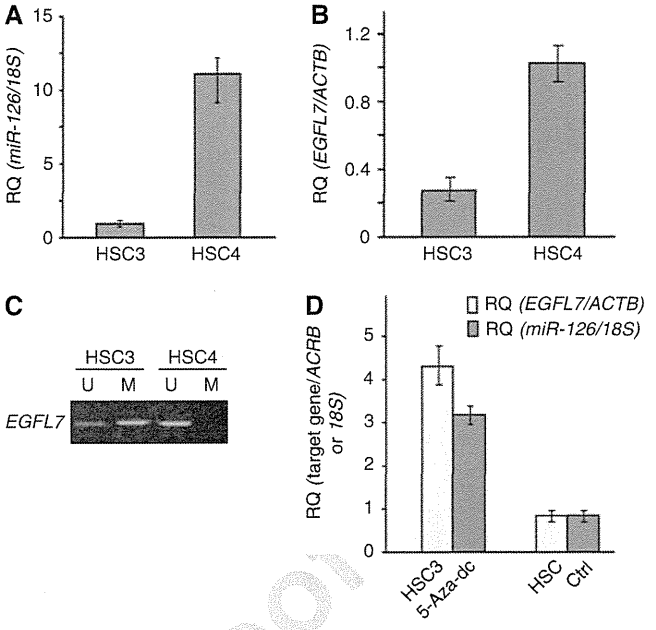

Figure 1 Expression levels of *miR-126* (**A**) and *EGFL7* (**B**) measured using qRT–PCR in the OSCC cells. The *18S* or beta-actin (*ACTB*) transcript levels were used as internal controls for *miR-126* and *EGFL7* expressions, respectively. The methylation status of *EGFL7* by MSP in the OSCC cells is shown in (**C**). The changes of the *miR-126* and *EGFL7* expressions in the 5-Aza-dc-treated HSC3 cells are shown in (**D**). The expression levels of *miR-126* and *EGFL7* in the untreated HSC3 cells were set to 1.

was absent in the HSC4 cells (Figure 1C). We next investigated the possibility that demethylation treatment could upregulate the *miR-126* and *EGFL7* expressions in the HSC3 cells. The treatment with 5-Aza-dc restored the expressions of *miR-126* and *EGFL7* (Figure 1D), whereas the expression levels of *miR-126* was not changed by TSA treatment (data not shown).

Functional analysis of miR-126 in the OSCC cells

The role of *miR-126* in OSCC progression was investigated using a functional analysis. The growth of HSC3 cells treated with pre-*miR-126* was inhibited in comparison with that of cells treated with control pre-*miR*. However, the growth of the HSC4 cells treated with an anti-*miR-126* inhibitor was restored compared with that of the cells treated with the control anti-miR inhibitor (Figure 2A). The number of invading cells was not affected by the treatment with pre-*miR-126* in the HSC3 cells or anti-*miR-126* in the HSC4 cells, in contrast to the number of cells treated with the control miR (Figure 2B). No significant changes in TUNEL-positive cells and caspase-3 activity were observed between the pre-*miR-126*-treated HSC3 cells or the anti-*miR-126*-treated HSC4 cells and the control-treated HSC3 or HSC4 cells (Figures 2C and D).

Changes in the VEGF expression levels in the OSCC cells treated with anti-miR-126 or pre-miR-126

As *VEGF-A* has been suggested to be negatively or positively regulated by *miR-126* (Fish *et al*, 2008; Liu *et al*, 2009; Zhu *et al*, 2011), we examined the effect of *miR-126* on the *VEGF-A*, *VEGF-C*, and *VEGF-D* expressions in the OSCC cells (Figure 3). Exposure to pre-*miR-126* increased *miR-126* expression but did not affect the *VEGF-C* and *VEGF-D* expression levels in the HSC3 cells, whereas the treatment with anti-*miR-126* inhibitor decreased the *miR-126* expression but not the *VEGF-C* and *VEGF-D* expressions in the HSC4 cells. However, induction of *miR-126* in the HSC3 cells and

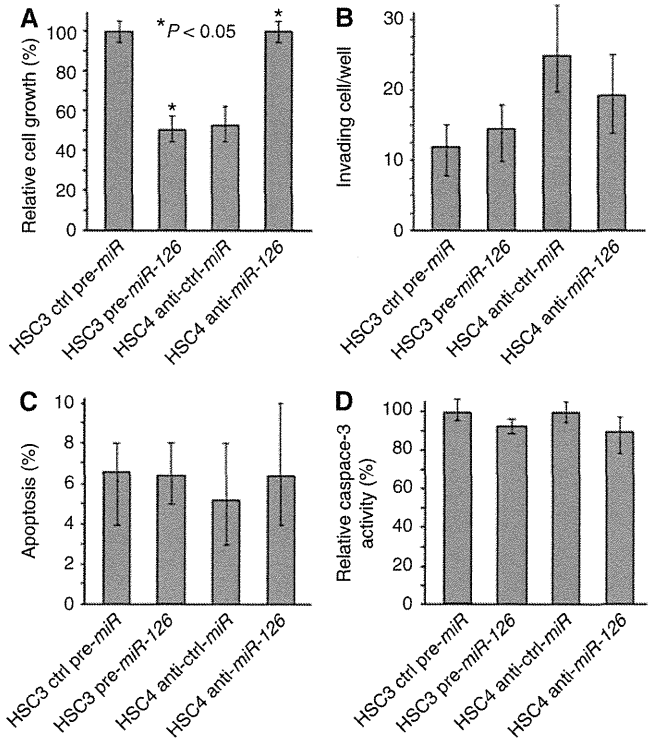

Figure 2 Functional analysis of *miR-126* in the OSCC cells. Cell growth (**A**), invasion (**B**), ratio of TUNEL-positive cells (**C**), and activity of caspase-3 (**D**) in the HSC3 or HSC4 cells treated with a *miR-126* precursor or anti-*miR-126*, respectively. Statistical significance was calculated by the Mann–Whitney *U*-test.

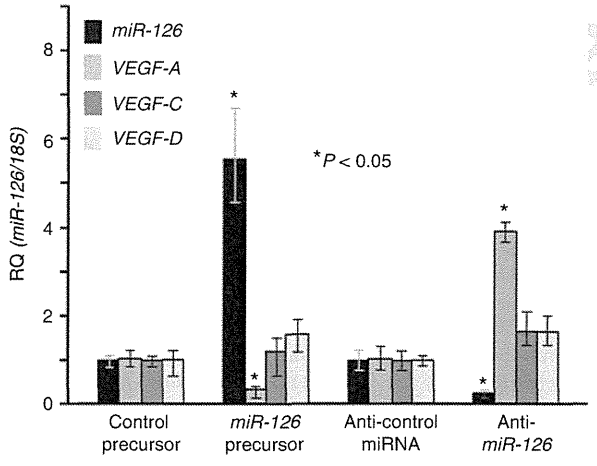

Figure 3 Effect of the *miR-126*, *VEGF-A*, *VEGF-C*, and *VEGF-D* expression levels in the OSCC cells treated with anti-*miR-126* or the *miR-126* precursor. The expression levels in the control miRNA precursor-treated HSC3 cells and the control anti-miRNA-treated HSC4 cells were set to 1. Statistical significance was determined using the Mann–Whitney *U*-test.

reduction of *miR-126* in the HSC4 cells were associated with the downregulation and the upregulation of *VEGF-A* expression, respectively. This was verified by the co-transfection of the *VEGF-A* wild-type 3′-UTR with pre-*miR-126*, which decreased luciferase activity, whereas this effect was completely ablated by deletion of the *miR-126*-binding site in the *VEGF-A* 3′-UTR (data not shown). These results suggested that *miR-126* acts as a negative regulator of *VEGF-A*, but not of *VEGF-C* and *VEGF-D*.

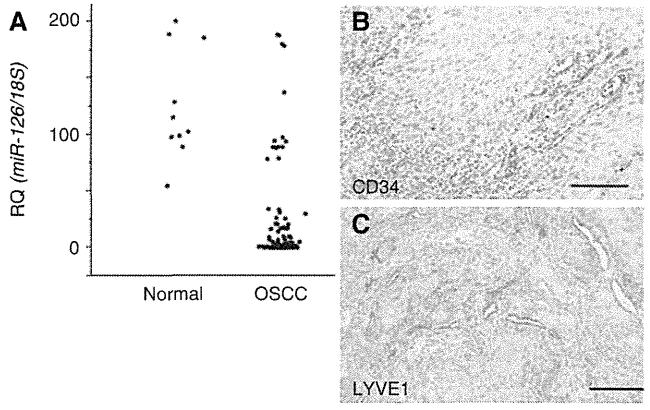

Figure 4 Expression levels of *miR-126* in OSCC compared with that in the normal oral mucosa (**A**) and MVD (**B**) or LVD (**C**) by immunohistochemistry. MVD and LVD were assessed according to the number of anti-CD34 and anti-LYVE1-positive vessels. Scale bar, 100 μm.

Relationship between the miR-126 expression and the clinicopathological characteristics in the OSCC specimens

MicroRNA-126 (*MiR-126*) expression was examined by qRT–PCR in the 118 cases with OSCC. The expression levels of *miR-126* in almost all the OSCC cases were low in comparison with the normal oral mucosa (Figure 4A). The *miR-126* expression and the clinicopathological characteristics in the OSCC specimens are summarised in Table 1. Ninety-four of the 118 OSCC samples (79.7%) showed low expression of *miR-126*. In the cases with local progression (T3 and T4), the expression levels of *miR-126* were significantly lower than those in the T1 and T2 cases ($P=0.036$). Low *miR-126* expression was detected in 52 (70.3%) of the 74 cases with early clinical-stage disease (stages I and II) and in 42 (95.5%) of the 44 cases with advanced clinical-stage disease (stages III and IV; $P=0.0006$). Although downregulation of *miR-126* was observed in 100% (34 out of 34) of the nodal metastasis-positive cases, 71.4% (60 out of 84) of the cases without nodal metastasis showed low expression of *miR-126* ($P<0.0001$). No significant correlation was found between the expression levels of *miR-126* and age, sex, site, or histological differentiation.

On the basis of the *in vitro* results showing that *miR-126* is a negative regulator of *VEGF-A*, we verified the relationship between *miR-126* and angiogenesis and lymphangiogenesis in OSCC (Table 2). A significant inverse correlation was observed between the *miR-126* expression levels and MVD ($P<0.0001$; Figure 4B) or LVD ($P<0.0001$; Figure 4D).

Relation between the miR-126 expression and the disease-free survival, and the prognosis of OSCCs

Local and nodal recurrence occurred in 44 of the 118 cases. The disease-free survival analysis of the OSCC patients revealed that a poor prognosis was associated with low *miR-126* expression compared with high *miR-126* expression cases ($P=0.0013$; Figure 5). The univariate analysis using the log-rank test indicated that the histological differentiation ($P=0.0022$), the clinical stage ($P=0.0015$), the nodal metastasis ($P<0.0001$), and the *miR-126* expression levels ($P=0.0006$) were associated with the poor outcome in OSCCs (Table 3). The multivariate analysis using the Cox proportional hazards model showed that nodal metastasis ($P=0.0093$) and *miR-126* expression levels ($P=0.048$) were prognostic factors for disease-free survival periods (Table 3).

Table 1 Relationship between the *miR-126* expressions and the clinicopathological parameters

Parameters	*miR-126* Low	*miR-126* High	*P*-value
Sex			
Male	52	16	
Female	42	8	0.1573
Age			
⩽65	34	12	
>65	60	12	0.221
Site			
Tongue	48	16	
Other	46	8	0.1268
Histological differentiation			
Well	56	14	
Mod, Poor	38	10	0.5451
T classification			
T1–T2	68	22	
T3–T4	26	2	0.036
Clinical stage			
I, II	52	22	
III, IV	42	2	0.0006
Nodal metastasis			
Negative	60	24	
Positive	34	0	<0.0001

Abbreviations: miR-126 = microRNA-126; Well = well-differentiated squamous cell carcinoma; Mod = moderately differentiated squamous cell carcinoma; Poor = poorly differentiated squamous cell carcinoma. The statistical analysis was performed by Fischer's exact *t*-test. The T classification and the clinical stage were performed according to the TNM classification.

Table 2 Relationship between the miR-126 expressions and angiogenesis or lymphangiogenesis

Parameter	miR-126 Low	miR-126 High	*P*-value
MVD	25.5761 ± 10.1091	11.0231 ± 4.6017	<0.0001
LVD	25.4468 ± 10.0379	10.3167 ± 4.014	<0.0001

Abbreviations: miR-126 = microRNA-126; ANOVA = analysis of variance. The statistical analysis was performed by one-factor ANOVA. Means ± s.d., each s.d. was less than 10%.

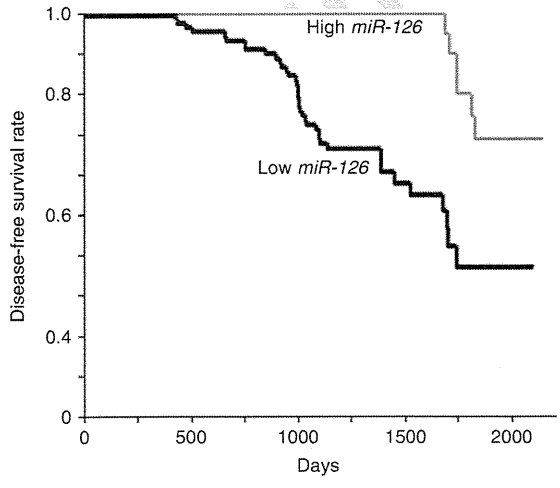

Figure 5 Disease-free survival curves of the OSCC patients calculated using the Kaplan–Meier method. Disease-free survival was analysed in correlation to the expression levels of *miR-126*. The miR-126-high cases ($n = 24$, event and censored data were 6 and 18, respectively), miR-126-low cases ($n = 94$, event and censored data were 38 and 56, respectively).

Table 3 Univariate and multivariate analysis of disease-free survival

Parameters	Risk ratio	95% CI	*P*-value
Univariate analysis			
Age			
⩽65	1		
>65	0.7672	0.4227–1.3998	0.3839
Gender			
Male	1		
Female	0.8843	0.4873–1.6304	0.6885
Site			
Tongue	1		
Other	0.9075	0.4927–1.6449	0.750
Histology			
Well	1		
Mod/Poor	2.4833	1.3989–4.7785	**0.0022**
T classification			
T1-T2	1		
T3-T4	1.4582	0.7206–2.759	0.2805
Clinical stage			
I, II	1		
III, IV	2.6417	1.4539–4.8528	**0.0015**
Nodal metastasis			
Negative	1		
Positive	4.7203	2.5653–8.7999	**<0.0001**
MVD			
Low	1		
High	1.0094	0.9827–1.0357	0.4872
LVD			
Low	1		
High	0.8492	0.4444–1.5712	0.607
miR-126			
High	1		
Low	4.0492	1.7558–11.0409	**0.0006**
Multivariate analysis			
Histology			
Well	1		
Mod, Poor	0.6673	0.3493–1.2557	0.2101
Clinical stage			
I, II	1		
III, IV	1.8972	0.9434–3.8782	**0.0725**
Nodal metastasis			
Negative	1		
Positive	2.6265	1.2658–5.6413	**0.0093**
miR-126			
High	1		
Low	2.631	0.9886–7.9851	**0.048**

Abbreviations: miR-126 = microRNA-126; CI = confidence intervals; Well = well-differentiated squamous cell carcinoma; Mod = moderately differentiated squamous cell carcinoma; Poor = poorly differentiated squamous cell carcinoma. The univariate analysis was performed by log-rank test, and the multivariate analysis was performed by the Cox proportional hazard model.

DISCUSSION

The present results show that *miR-126* is a negative regulator of *VEGF-A* and promotes cell growth in OSCC cells. In addition, the decreased *miR-126* expression was associated with the induction of tumoural angiogenesis and lymphangiogenesis, tumour

progression, nodal metastasis, and poor prognosis in the OSCC cases. The HSC3 cells are human OSCC-derived metastatic cells, whereas the HSC4 cells have low metastatic potential (Momose *et al*, 1989; Sasahira *et al*, 2007a; Sasahira *et al*, 2008; Sasahira *et al*, 2010). The HSC3 cells are characterised by adhesion to type-IV collagen, colony formation in a type-I collagen matrix (Momose *et al*, 1989), high heparanase activity (Ikuta *et al*, 2001), reduction of *nm23H1* expression and upregulated matrix metalloproteinase (*MMP)-2/MMP-9* (Khan *et al*, 2001), and higher expression of *VEGF-A/C/D* in comparison with HSC4 cells. In this study, the HSC3 cells showed lower expression of *miR-126* compared with the HSC4 cells, and the decrease of *miR-126* activity might be associated with a higher capacity for lymph node metastasis in these cells. Further investigation of the expression levels of *miR-126* in OSCC may help predict the tendency for lymph node metastasis development in this type of malignancy. Vascular endothelial growth factor (*VEGF*)-*A* is a potent trigger for tumoural angiogenesis (Stockmann *et al*, 2008); however, we previously reported that *VEGF-A* induces not only angiogenesis but also lymphangiogenesis, and *VEGF-A*-dependent angiogenesis and lymphangiogenesis accelerate local progression, nodal metastasis, and recurrence of OSCC (Sasahira *et al*, 2010). This is in agreement with previous studies that demonstrated a strong correlation between *VEGF-A* expression and tumour progression (Takahashi *et al*, 1995), worse prognosis (Maeda *et al*, 1996), and lymph node metastasis via induction of lymphangiogenesis (Nagy *et al*, 2002; Hirakawa *et al*, 2005). Further examination will help reveal the mechanism underlying the role of *miR-126* and *VEGF-A*-related angiogenesis and lymphangiogenesis in tumour progression.

MicroRNA-126 (*MiR-126*) is an endothelial-specific *miRNA* that is located within intron 7 of *EGFL7* (Fish *et al*, 2008; Wang *et al*, 2008a). An intronic *miRNA* tends to be co-expressed with its host gene (Baskerville and Bartel, 2005; Saito *et al*, 2009), and a previous report showed that *miR-126* and its host gene, *EGFL7*, are downregulated by DNA methylation, with restoration of expression levels by epigenetic treatment (Saito *et al*, 2009). We also observed decreased expression and methylation of *EGFL7* in the highly metastatic OSCC cell line HSC3 compared with the HSC4 cell line with lower metastasis. In addition, *EGFL7* and *miR-126* recovered normal expression levels in response to the 5-Aza-dc treatment in the HSC3 cells. Further examination of *miR-126* might reveal this molecule as a useful target for epigenetic therapy in progressive and metastatic OSCC.

MicroRNAs are well preserved in formalin-fixed, paraffin-embedded (FFPE) specimens owing to the small size of the RNA (Xi *et al*, 2007; Donnem *et al*, 2011). Most of the previous reports on *miR-126* expression were based on the analysis of frozen tissues containing non-tumour cells or tumour stromal cells including vessels (Wang *et al*, 2008b; Saito *et al*, 2009; Liu *et al*, 2009; Feng *et al*, 2010; Otsubo *et al*, 2011; Zhu *et al*, 2011). However, *miR-126* is a positive regulator of angiogenesis in normal endothelial cells (Fish *et al*, 2008; Wang *et al*, 2008a; Liu *et al*, 2009; Miko *et al*, 2011; Zhu *et al*, 2011). In vasculogenesis, which is not associated with cancer, such as in wound healing, overexpression of *miR-126* in endothelial cells enhances *VEGF-A* activity and promotes vessel formation by repressing the expression of sprouty-related protein-1 (*Spred-1*; Wang *et al*, 2008a). Sprouty-related protein-1 (*spred-1*) is an intracellular inhibitor of angiogenic signals (Wang *et al*, 2008a). As *VEGF-A* is not a direct target of *miR-126* in endothelial cells, the use of fresh frozen samples, including stromal cells, may lead to an incorrect interpretation of results. We therefore selected OSCC cells using the LCM technique in FFPE tissues and performed the expression analysis of *miR-126* by real-time RT–PCR. We also confirmed the increased *miR-126* expression and the decreased *Spred-1* expression in the microdissected endothelial cells by qRT–PCR (data not shown).

In conclusion, the present results demonstrate that low *miR-126* expression is correlated with tumour progression through the activation of angiogenesis and lymphangiogenesis in OSCC. However, the exact mechanism underlying the *miR-126*-mediated activation of angiogenesis and lymphangiogenesis remains to be elucidated. *In vivo* studies will be helpful in the future to further clarify this mechanism. Our results suggest that re-expression of *miR-126* could be a useful therapeutic strategy against human OSCC.

ACKNOWLEDGEMENTS

This work was supported in part by a Grant-in-Aid for Scientific Research from the Japan Society for the Promotion of Science, Japan.

Conflict of Interest

The authors declare no conflict of interest.

REFERENCES

Adams RH, Alitalo K (2007) Molecular regulation of angiogenesis and lymphangiogenesis. *Nat Rev Mol Cell Biol* **8**(6): 464–478

Argiris A, Karamouzis MV, Raben D, Ferris RL (2008) Head and neck cancer. *Lancet* **371**: 1695–1709

Bartel DP (2009) MicroRNAs: target recognition and regulatory functions. *Cell* **136**(2): 215–233

Baskerville S, Bartel DP (2005) Microarray profiling of microRNAs reveals frequent coexpression with neighboring miRNAs and host genes. *RNA* **11**(3): 241–247

Calin GA, Croce CM (2006) MicroRNA signatures in human cancers. *Nat Rev Cancer* **6**(11): 857–866

Carmeliet P (2005) Angiogenesis in life, disease and medicine. *Nature* **438**(7070): 932–936

Currie MJ, Hanrahan V, Gunningham SP, Morrin HR, Frampton C, Han C, Robinson BA, Fox SB (2004) Expression of vascular endothelial growth factor D is associated with hypoxia inducible factor (HIF-1alpha) and the HIF-1alpha target gene DEC1, but not lymph node metastasis in primary human breast carcinomas. *J Clin Pathol* **57**(8): 829–834

Donnem T, Al-Shibli K, Al-Saad S, Delghandi MP, Busund LT, Bremnes RM (2009) VEGF-A and VEGFR-3 correlate with nodal status in operable non-small cell lung cancer: inverse correlation between expression in tumor and stromal cells. *Lung Cancer* **63**(2): 277–283

Donnem T, Fenton CG, Lonvik K, Berg T, Eklo K, Andersen S, Stenvold H, Al-Shibli K, Al-Saad S, Bremnes RM, Busund LT (2012) MicroRNA signatures in tumor tissue related to angiogenesis in non-small cell lung cancer. *PLos One* **7**(1): e29671

Donnem T, Lonvik K, Eklo K, Berg T, Sorbye SW, Al-Shibli K, Al-Saad S, Andersen S, Stenvold H, Bremnes RM, Busund LT (2011) Independent and tissue-specific prognostic impact of miR-126 in nonsmall cell lung cancer: coexpression with vascular endothelial growth factor-A predicts poor survival. *Cancer* **117**(14): 3193–3200

Dos Reis PP, Bharadwaj RR, Machado J, Macmillan C, Pintilie M, Sukhai MA, Perez-Ordonez B, Gullane P, Irish J, Kamel-Reid S (2008) Claudin 1 overexpression increases invasion and is associated with aggressive histological features in oral squamous cell carcinoma. *Cancer* **113**(11): 3169–3180

Feng R, Chen X, Yu Y, Su L, Yu B, Li J, Cai Q, Yan M, Liu B, Zhu Z (2010) miR-126 functions as a tumour suppressor in human gastric cancer. *Cancer Lett* **298**(1): 50–63

Fish JE, Santoro MM, Morton SU, Yu S, Yeh RF, Wythe JD, Ivey KN, Bruneau BG, Stainier DY, Srivastava D (2008) miR-126 regulates angiogenic signaling and vascular integrity. *Dev Cell* **15**(2): 272–284

Hirakawa S, Kodama S, Kunstfeld R, Kajiya K, Brown LF, Detmar M (2005) VEGF-A induces tumor and sentinel lymph

node lymphangiogenesis and promotes lymphatic metastasis. *J Exp Med* **201**(7): 1089–1099

Ikuta M, Podyma KA, Maruyama K, Enomoto S, Yanagishita M (2001) Expression of heparanase in oral cancer cell lines and oral cancer tissues. *Oral Oncol* **37**(2): 177–184

Jemal A, Bray F, Center MM, Ferlay J, Ward E, Forman D (2011) Global cancer statistics. *CA Cancer J Clin* **61**(2): 69–90

Jiao LR, Frampton AE, Jacob J, Pellegrino L, Krell J, Giamas G, Tsim N, Vlavianos P, Cohen P, Ahmad R, Keller A, Habib NA, Stebbing J, Castellano L (2012) MicroRNAs targeting oncogenes are down-regulated in pancreatic malignant transformation from benign tumors. *PLos One* **7**(2): e32068

Khan MH, Yasuda M, Higashino F, Haque S, Kohgo T, Nakamura M, Shindoh M (2001) nm23-H1 suppresses invasion of oral squamous cell carcinoma-derived cell lines without modifying matrix metalloproteinase-2 and matrix metalloproteinase-9 expression. *Am J Pathol* **158**(5): 1785–1791

Kitano M, Rahbari R, Patterson EE, Xiong Y, Prasad NB, Wang Y, Zeiger MA, Kebebew E (2011) Expression profiling of difficult-to-diagnose thyroid histologic subtypes shows distinct expression profiles and identify candidate diagnostic microRNAs. *Ann Surg Oncol* **18**(12): 3443–3452

Liu B, Peng XC, Zheng XL, Wang J, Qin YW (2009) MiR-126 restoration down-regulate VEGF and inhibit the growth of lung cancer cell lines in vitro and in vivo. *Lung Cancer* **66**(2): 169–175

Liu X, Sempere LF, Ouyang H, Memoli VA, Andrew AS, Luo Y, Demidenko E, Korc M, Shi W, Preis M, Dragnev KH, Li H, Direnzo J, Bak M, Freemantle SJ, Kauppinen S, Dmitrovsky E (2010) MicroRNA-31 functions as an oncogenic microRNA in mouse and human lung cancer cells by repressing specific tumor suppressors. *J Clin Invest* **120**(4): 1298–1309

Maeda K, Chung YS, Ogawa Y, Takatsuka S, Kang SM, Ogawa M, Sawada T, Sowa M (1996) Prognostic value of vascular endothelial growth factor expression in gastric carcinoma. *Cancer* **77**(5): 858–863

Marsh D, Suchak K, Moutasim KA, Vallath S, Hopper C, Jerjes W, Upile T, Kalavrezos N, Violette SM, Weinreb PH, Chester KA, Chana JS, Marshall JF, Hart IR, Hackshaw AK, Piper K, Thomas GJ (2011) Stromal features are predictive of disease mortality in oral cancer patients. *J Pathol* **223**(4): 470–481

Martello G, Rosato A, Ferrari F, Manfrin A, Cordenonsi M, Dupont S, Enzo E, Guzzardo V, Rondina M, Spruce T, Parenti AR, Daidone MG, Bicciato S, Piccolo S (2010) A MicroRNA targeting dicer for metastasis control. *Cell* **141**(7): 1195–1207

Meister J, Schmidt MH (2010) miR-126 and miR-126*: new players in cancer. *Sci World J* **10**: 2090–2100

Miko E, Margitai Z, Czimmerer Z, Varkonyi I, Dezso B, Lanyi A, Bacso Z, Scholtz B (2011) miR-126 inhibits proliferation of small cell lung cancer cells by targeting SLC7A5. *FEBS Lett* **585**(8): 1191–1196

Momose F, Araida T, Negishi A, Ichijo H, Shioda S, Sasaki S (1989) Variant sublines with different metastatic potentials selected in nude mice from human oral squamous cell carcinomas. *J Oral Pathol Med* **18**(7): 391–395

Mydlarz WK, Hennessey PT, Califano JA (2010) Advances and perspectives in the molecular diagnosis of head and neck cancer. *Expert Opin Med Diagn* **4**(1): 53–65

Nagy JA, Vasile E, Feng D, Sundberg C, Brown LF, Detmar MJ, Lawitts JA, Benjamin L, Tan X, Manseau EJ, Dvorak AM, Dvorak HF (2002) Vascular permeability factor/vascular endothelial growth factor induces lymphangiogenesis as well as angiogenesis. *J Exp Med* **196**(11): 1497–1506

Nomiya T, Nemoto K, Nakata E, Takai Y, Yamada S (2006) Expression of thymidine phosphorylase and VEGF in esophageal squamous cell carcinoma. *Oncol Rep* **15**(6): 1497–1501

Miyahara M, Tanuma J, Sugihara K, Semba I (2007) Tumor lymphangiogenesis correlates with lymph node metastasis and clinicopathologic parameters in oral squamous cell carcinoma. *Cancer* **110**(6): 1287–1294

Moriyama M, Kumagai S, Kawashiri S, Kojima K, Kakihara K, Yamamoto E (1997) Immunohistochemical study of tumour angiogenesis in oral squamous cell carcinoma. *Oral Oncol* **33**(5): 369–374

Otsubo T, Akiyama Y, Hashimoto Y, Shimada S, Goto K, Yuasa Y (2011) MicroRNA-126 inhibits SOX2 expression and contributes to gastric carcinogenesis. *PLoS One* **6**(1): e16617

Saito Y, Friedman JM, Chihara Y, Egger G, Chuang JC, Liang G (2009) Epigenetic therapy upregulates the tumor suppressor microRNA-126 and its host gene EGFL7 in human cancer cells. *Biochem Biophys Res Commun* **379**(3): 726–731

Sasahira T, Kirita T, Bhawal UK, Ikeda M, Nagasawa A, Yamamoto K, Kuniyasu H (2007a) The expression of receptor for advanced glycation end products is associated with angiogenesis in human oral squamous cell carcinoma. *Virchows Arch* **450**(3): 287–295

Sasahira T, Kirita T, Bhawal UK, Yamamoto K, Ohmori H, Fujii K, Kuniyasu H (2007b) Receptor for advanced glycation end products (RAGE) is important in the prediction of recurrence in human oral squamous cell carcinoma. *Histopathology* **51**(2): 166–172

Sasahira T, Kirita T, Kurihara M, Yamamoto K, Bhawal UK, Bosserhoff AK, Kuniyasu H (2010) MIA-dependent angiogenesis and lymphangiogenesis are closely associated with progression, nodal metastasis and poor prognosis in tongue squamous cell carcinoma. *Eur J Cancer* **46**(12): 2285–2294

Sasahira T, Kirita T, Oue N, Bhawal UK, Yamamoto K, Fujii K, Ohmori H, Luo Y, Yasui W, Bosserhoff AK, Kuniyasu H (2008) High mobility group box-1-inducible melanoma inhibitory activity is associated with nodal metastasis and lymphangiogenesis in oral squamous cell carcinoma. *Cancer Sci* **99**(9): 1806–1812

Siegel R, Naishadham D, Jemal A (2012) Cancer statistics, 2012. *Cancer J Clin* **62**(1): 10–29

Slaby O, Redova M, Poprach A, Nekvindova J, Iliev R, Radova L, Lakomy R, Svoboda M, Vyzula R (2012) Identification of MicroRNAs associated with early relapse after nephrectomy in renal cell carcinoma patients. *Genes Chromosomes Cancer* **51**(7): 707–716

Stockmann C, Doedens A, Weidemann A, Zhang N, Takeda N, Greenberg JI, Cheresh DA, Johnson RS (2008) Deletion of vascular endothelial growth factor in myeloid cells accelerates tumorigenesis. *Nature* **456**(7223): 814–818

Takahashi Y, Kitadai Y, Bucana CD, Cleary KR, Ellis LM (1995) Expression of vascular endothelial growth factor and its receptor, KDR, correlates with vascularity, metastasis, and proliferation of human colon cancer. *Cancer Res* **55**(18): 3964–3968

Wang S, Aurora AB, Johnson BA, Qi X, McAnally J, Hill JA, Richardson JA, Bassel-Duby R, Olson EN (2008a) The endothelial-specific microRNA miR-126 governs vascular integrity and angiogenesis. *Dev Cell* **15**(2): 261–271

Wang X, Tang S, Le SY, Lu R, Rader JS, Meyers C, Zheng ZM (2008b) Aberrant expression of oncogenic and tumor-suppressive microRNAs in cervical cancer is required for cancer cell growth. *PLoS One* **3**(7): e2557

Watahiki A, Wang Y, Morris J, Dennis K, O'Dwyer HM, Gleave M, Gout PW, Wang Y (2011) MicroRNAs associated with metastatic prostate cancer. *PLoS One* **6**(9): e24950

Watanabe K, Emoto N, Hamano E, Sunohara M, Kawakami M, Kage H, Kitano K, Nakajima J, Goto A, Fukayama M, Nagase T, Yatomi Y, Ohishi N, Takai D (2012) Genome structure-based screening identified epigenetically silenced microRNA associated with invasiveness in non-small-cell lung cancer. *Int J Cancer* **130**(11): 2580–2590

Xi Y, Nakajima G, Gavin E, Morris CG, Kudo K, Hayashi K, Ju J (2007) Systematic analysis of microRNA expression of RNA extracted from fresh frozen and formalin-fixed paraffin-embedded samples. *RNA* **13**(10): 1668–1674

Yu T, Wang XY, Gong RG, Li A, Yang S, Cao YT, Wen YM, Wang CM, Yi XZ (2009) The expression profile of microRNAs in a model of 7,12-dimethyl-benz[a]anthrance-induced oral carcinogenesis in Syrian hamster. *J Exp Clin Cancer Res* **2009**(28): 64

Zhu N, Zhang D, Xie H, Zhou Z, Chen H, Hu T, Bai Y, Shen Y, Yuan W, Jing Q, Qin Y (2011) Endothelial-specific intron-derived miR-126 is down-regulated in human breast cancer and targets both VEGFA and PIK3R2. *Mol Cell Biochem* **351**(1-2): 157–164

Zhu X, Li H, Long L, Hui L, Chen H, Wang X, Shen H, Xu W (2012) miR-126 enhances the sensitivity of non-small cell lung cancer cells to anticancer agents by targeting vascular endothelial growth factor A. *Acta Biochim Biophys Sin* **44**(6): 519–526

tapraid2/zr5-uro/zr5-uro/zr599908/zr50690d08z | nairre | S=1 | 6/10/10 | 5:21 | Art: 6839 | ce: 19

ELSEVIER

Urologic Oncology: Seminars and Original Investigations xx (2010) xxx

UROLOGIC ONCOLOGY

Original article

High matrix metalloproteinase-to-E-cadherin ratio measured by bicolor fluorescent in situ hybridization is associated with lymphangiogenesis and lymph node metastasis in prostate cancer☆

Yi Luo, M.D.[a], Hitoshi Ohmori, M.D., Ph.D.[a], Kiyomu Fujii, M.D., Ph.D.[a], Yoshitomo Chihara, M.D., Ph.D.[a], Satoshi Maruyama, M.D., Ph.D.[b], Hiroki Kuniyasu, M.D., Ph.D.[a,*]

[a] *Department of Molecular Pathology, Nara Medical University, Kashihara, Japan*
[b] *Department of Urology, Miyoshi Central Hospital, Miyoshi, Japan*

Received 14 January 2010; received in revised form 8 April 2010; accepted 3 May 2010

Abstract

Objective: The colorimetric in situ hybridization (CISH)-based matrix metalloproteinase (MMP)-to-E-cadherin (ECD) ratio (MER) has been revealed as an excellent marker for the disease stage in prostate cancer. The one aim of this study was investigating a new method for estimation of MER by bicolor fluorescent ISH (bicolor FISH) with a computerized fluorescence detector-based system. Another aim was examination of relation of MER by bicolor FISH with expression of vascular endothelial growth factor-C (VEGF-C).

Methods: The bicolor FISH technique used cyanin 5 (cy5)-labeled MMP-2 and −9 probes, and a cyanin 3 (cy3)-labeled ECD probe on needle biopsy specimens from 67 prostate cancer cases. The ISH was followed by computerized detection of the signal intensities and cy5-to-cy3 ratios using a fluorescence detector. VEGF-C expression was examined using cy5-labeled VEGF-C by computerized detection.

Results: The bicolor FISH-based MER was well correlated with CISH-based MER ($P < 0.0001$). The bicolor FISH-based MER correlated with Gleason score and pathologic stage of the cases. VEGF-C mRNA expression was associated with the pathologic stage and maximum lymph vessel density (LVD). The LVD was associated with VEGF-C expression at the tumor area where the maximum MER was detected ($P < 0.0001$).

Conclusion: The MER was correlated with the VEGF-C expression and LVD, indicating lymph node metastasis of prostate cancer. Therefore, this computer-assisted MER is a useful marker for preoperative prediction of disease stage, especially lymph node metastasis, of prostate cancer. © 2010 Published by Elsevier Inc.

Keywords: Prostate cancer; Lymph node metastasis; MMP; E-cadherin; VEGF-C; FISH

1. Introduction

To preoperatively evaluate the disease progression and malignant potential of prostate cancer, digital palpation, radiological imaging studies, serum prostate-specific antigen (PSA), the biopsy Gleason score, and additional tumor-related information gained from prostatic core needle biopsy specimens are assessed [1–3]. The purpose for such assessments is to distinguish organ-confined disease from advanced cancer and non-metastasized diseases from metastasized ones.

We have previously reported the significance of the relative mRNA expression between matrix metalloproteinases (MMPs) and E-cadherin (ECD): the ratio of expressions of MMP-2 and MMP-9 to that of ECD (MMP-to-ECD ratio, or MER) has been shown to be well associated with extra-organ extension of prostate cancer by using an colorimetric in situ hybridization (CISH) technique on radical prostatectomy specimens [4] and prostatic core needle biopsy specimens [5]. A higher MER represents enhanced stromalysis and diminished cell-to-cell adhesion, which are thought to activate invasion and infiltration into vascular and/or lymphatic ducts [6,7].

☆This work was supported in part by a Grant-in-Aid for Scientific Research from Japan Society for the Promotion of Science, Japan.

* Corresponding author. Tel.: +81-744-22-3051; fax: +81-744-25-7308.

E-mail address: cooninh@zb4.so-net.ne.jp (H. Kuniyasu).

1078-1439/$ – see front matter © 2010 Published by Elsevier Inc.
doi:10.1016/j.urolonc.2010.05.001

tapraid2/zr5-uro/zr5-uro/zr599908/zr50690d08z | nairre | S=1 | 6/10/10 | 5:21 | Art: 6839 | ce: 19

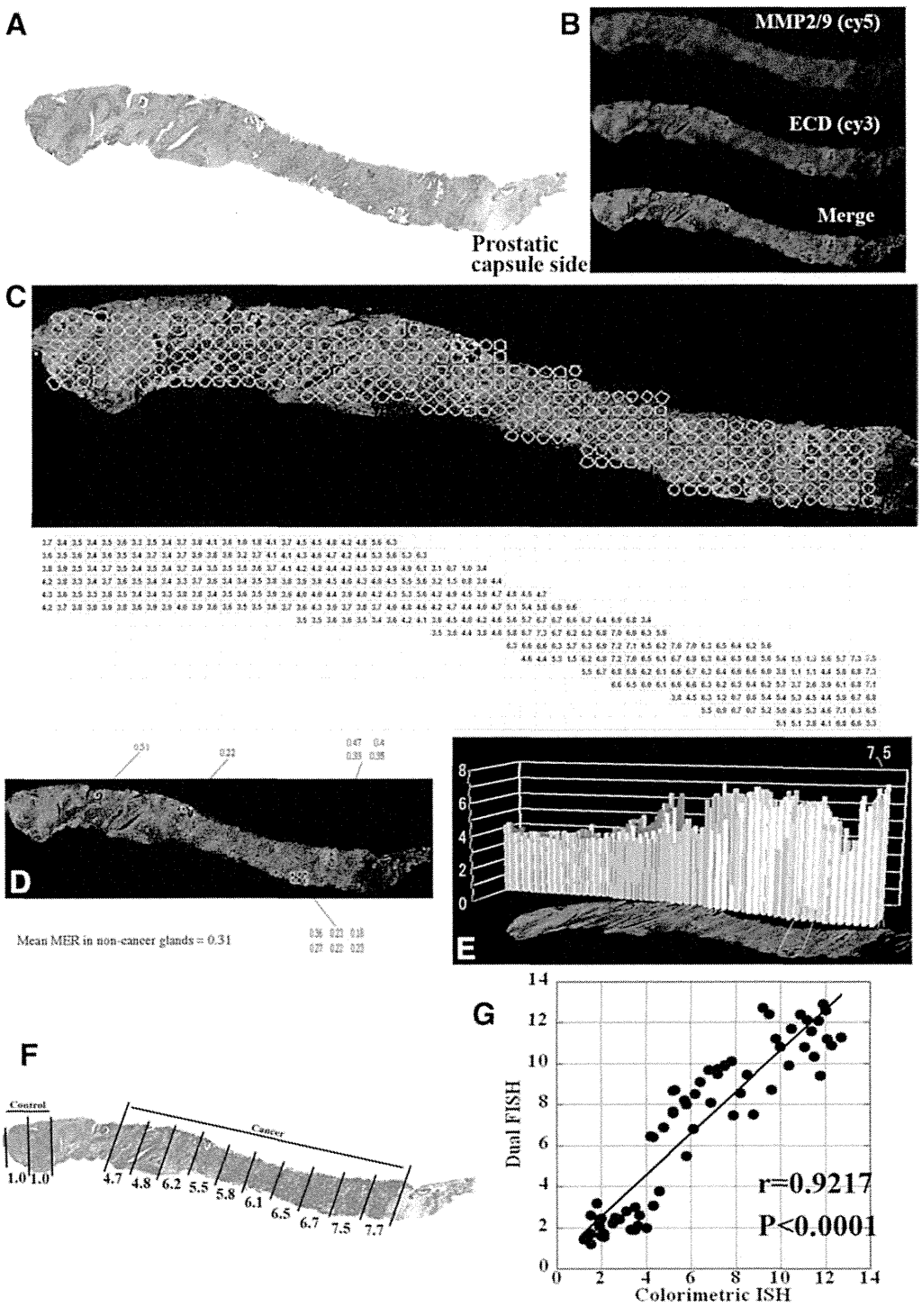

Fig. 1. Bicolor FISH technique. (A) Grey-scale image of a prostate core needle biopsy specimen captured by the fluorescent detector. The right side of the image directed a prostatic capsule side of the specimen. (B) Fluorescence images of ISH with cy5-labeled MMP-2 or MMP-9, cy3-labeled ECD, and the merged cy5–cy3 staining. (C) Setting of the measuring circles to determine the intensities of fluorescence. Measuring circles (50-μm diameter) were set to cover the whole specimen (upper panel). In each circle, the fluorescence intensities of cy5 and cy3 were designated as the ratio of cy5 to cy3 (lower panel). (D) Standardization to the signals of normal glands. The measuring circles covering normal glands were selected, and used as a built-in control for the expressions of MMP-2, MMP-9, and ECD. The mean cy5-to-cy3 ratio was calculated from the measuring circles covering the normal glands. The cy5-to-cy3

tapraid2/zr5-uro/zr5-uro/zr599908/zr50690d08z | nairre | S=1 | 6/10/10 | 5:21 | Art: 6839 | ce: 19

Lymphangiogenesis is a key player in lymphatic cancer metastasis [8]. In prostate cancer, lymphangiogenesis is also important in lymph node metastasis [9]. Pelvic lymph node metastasis is closely associated with the worst prognosis for prostate cancer [10]. The aggressiveness of lymph node metastasis is inversely correlated with both survival rate and disease-free survival [11]. Several molecules reportedly enhance lymphangiogenesis [12]: vascular endothelial growth factor (VEGF)-C, VEGF-D, VEGF-A, platelet-derived growth factor (PDGF)-BB, hepatocyte growth factor, and melanoma inhibitory activity (MIA) attend to lymph vessel proliferation through activation of VEGF receptor-3, PDGF receptor, c-*met*, and integrins [11,13–15]. Especially, VEGF-C is a common lymphangiogenic factor in many human cancers [16]. It is one of our aims of the present study to investigate the relationships among lymphangiogenesis, VEGF-C, and disease progression. Lymphangiogenesis is assessed by lymphatic duct density (LVD) in tumor tissues [15]. The maximum LVD is also associated with the diameters of the lymphatic ducts. Our previous studies show MER is well associated with disease progression [4,5]. We then focused on the relationships among MER, lymphangiogenesis, and VEGF-C.

The CISH technique possesses some technical difficulties resulting from an observer-based error and a sampling error. In the present study, to resolve the problem we verified a new method to estimate the MER by using a bicolor fluorescent in situ hybridization (bicolor FISH) technique with a computerized fluorescence detector-based system. We then compared the computer-assisted MER with lymph node metastasis, lymph vessel density (LVD), and VEGF-C expression.

2. Materials and methods

2.1. Patient characteristics and histopathology

Formalin-fixed, paraffin-embedded biopsy specimens from 67 selected previously untreated patients at the Miyoshi Central Hospital (2004–2009) were examined. The cases was selected by the total cancer content, which was more than 2 mm in 6 to 10 specimens of the prostatic core biopsy to avoid misdiagnosis due to too small cancer amount according to our previous study [23]. The cases with cancer in other organ were excluded. The presence, extent, and grade of cancer were determined for the specimens by examining 4-μm-thick tissue sections stained for hematoxylin and eosin (H and E) light microscopy. The highest Gleason score sum was the value assigned to the specimens. Pathologic stage was assigned by using the 1997 tumor-node-metastasis (TNM) staging system [17] as follows: pT2, organ-confined cancer; pT3a,extraprostatic extension; pT3b, seminal vesicle invasion. As all patients exhibiting pelvic lymph node metastasis at surgery also exhibited extraprostatic extension of the primary tumor, the stage was assigned as pT3a or b with N+ (e.g., pT3a-b/N1).

2.2. Oligonucleotide probes

Specific antisense oligonucleotide DNA probes were designed and synthesized as reported previously [18]. The sequences and working dilution of the probes were as follows: MMP-9, 5′-CCG GTC CAC CTC GCT GGC GCT CCG GA-3′ (1:200); MMP-2, 5′-GGC CAC ATC TGG GTT GCG GC-3′ (1:200); ECD, mixture of 5′-TGG AGC GGG CTG GAG TCT GAA CTG-3′ (1:200) and 5′-GAC GCC GGC GGC CCC TTC ACA GTC-3′ (1:200); and VEGF-C, 5′- CGG GGC GGG GGA CAC CAG-3′ (1:100). For bicolor FISH, probes for MMP-9 and MMP-2 were conjugated with cyanin 5 (cy5) and probes for ECD was conjugated with cyanin 3 (cy3). VEGF-C was conjugated with cy5. For CISH, MMP2, MMP9, ECD, and poly$(dT)_{20}$ probes were conjugated with fluorescein isothiocyanate (FITC). A $(dT)_{20}$ oligonucleotide was used to verify the mRNA integrity in each sample for the CISH assay [18,19]. The lyophilized probes were reconstituted to 1 μg/μl of stock solution in 10-mM Tris-HCl (pH 7.6) and 1-mM EDTA. The stock solution was diluted with Probe Diluent (Research Genetics Inc., Huntsville, AL) immediately before use.

2.3. The ISH technique

ISH was performed as described previously [4,5,20] and carried out according to the microprobe manual staining system (Fisher Scientific, Pittsburgh, PA). Formalin-fixed, paraffin-embedded specimens (4-μm thickness) were mounted on silane-coated ProbeOn slides (Fisher Scientific). The preservation period of the tissue block was 3–56 months (median 23 month). The sectioned specimens were stored at 4°C in a humidiated refrigerator. The specimens were used for ISH within 3 weeks after thin section. The slides were placed in the microprobe slide holder, dewaxed, and dehydrated followed by enzymatic digestion with pepsin (8 g/l in 0.2-M HCl; DAKO Corp., Carpinteria, CA). Hybridization of the probe (0.05 μg/μl diluted with Probe Diluent) was carried out for 90 minutes at 45°C, and the samples were

ratios from measuring circles covering the tumor areas were standardized to the mean cy5-to-cy3 ratio, which was set to 1.0. (E) The MER is represented by the bar graph in relation to the merged histological appearance. (F) The measuring method of MER from CISH. The staining intensity by CISH was measured in each 1 mm-length area. The mean intensity values of MMP2, MMP9, and ECD was standardized by the intensity of poly-dT20 probe. The MER of each area was calculated according to the formula; (MMP2 + MMP9)/2 × ECD. (G) Comparison of dual FISH-based MER with CISH-based MER. r = Spearman's rho.

tapraid2/zr5-uro/zr5-uro/zr599908/zr50690d08z | nairre | S=1 | 6/10/10 | 5:21 | Art: 6839 | ce: 19

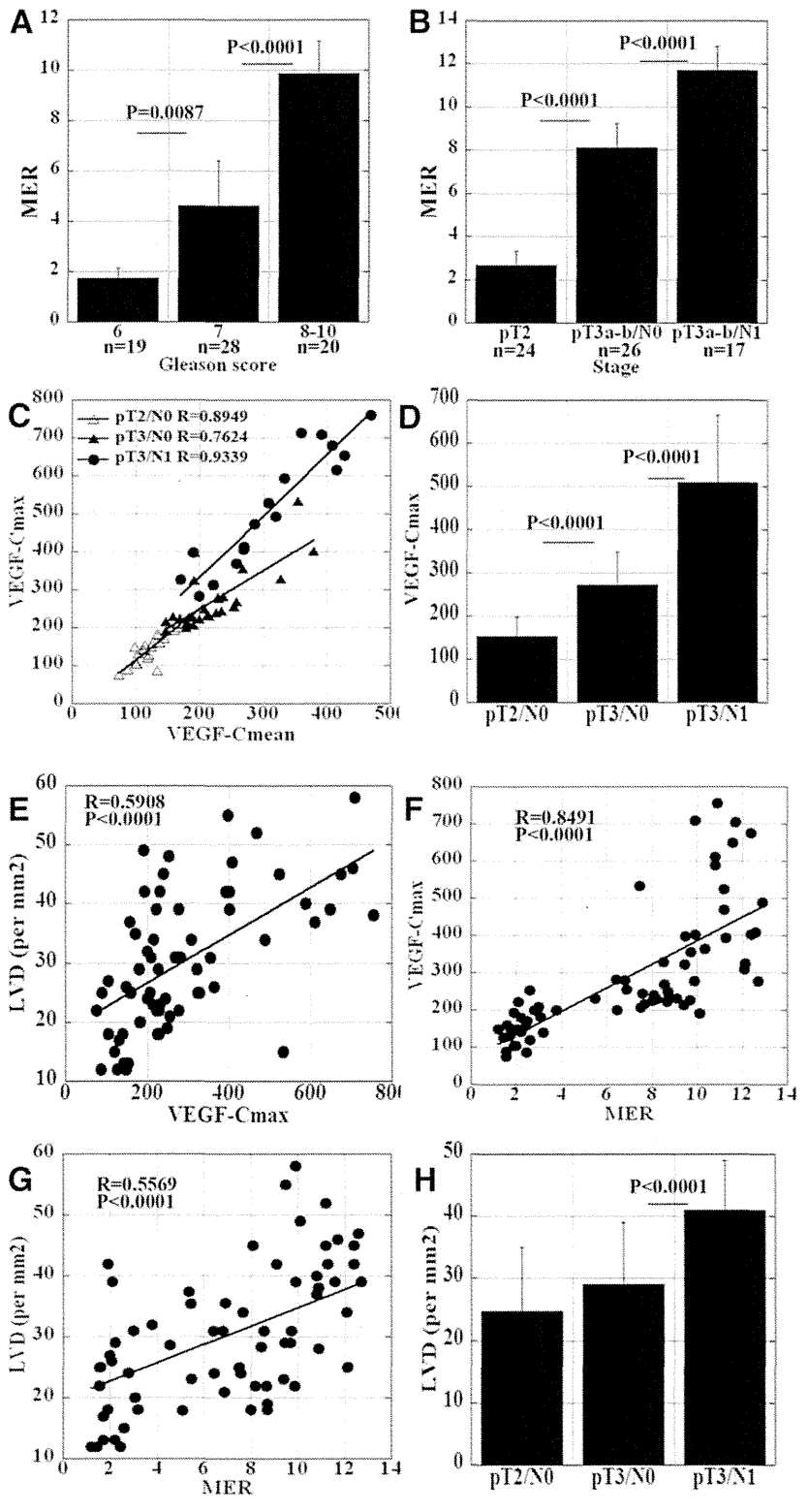

Fig. 2. The MER, VEGF-C expression, and LVD in the 67 prostate cancer cases. (A) Relation of the FISH-based MER to the Gleason score, (B) relation of the FISH-based MER to the pathologic stage, (C) correlation between the VEGF-C_{max} and VEGF-C_{mean}, (D) relation of the VEGF-C_{max} to the pathologic

tapraid2/zr5-uro/zr5-uro/zr599908/zr50690d08z | nairre | S=1 | 6/10/10 | 5:21 | Art: 6839 | ce: 19

then washed thrice with 1× saline-sodium citrate (SSC) buffer for 2 minutes at 45°C. The slides were covered with glass slips using ParmaFluoro (Research Genetics Inc.). For the bicolor FISH assay, hybridized specimens were examined by a computer-assisted image analyzer. For the CISH assay, the samples were incubated in alkaline phosphatase-labeled avidin for 30 minutes at 45°C, briefly rinsed in 50-mM Tris buffer (pH 7.6), rinsed with alkaline phosphatase enhancer (Biomedia Corp., Foster City, CA) for 1 minute, and finally incubated with chromogen substrate Fast Red (Research Genetics) for 30 minutes at 45°C.

2.4. Image analysis and the MER in bicolor FISH

For the bicolor FISH assay, a fluorescence detector (Genetix, New Milton, UK) and microarray analysis software (QuantArray; GSI Lumonics Inc., Northville, MI) were used (Fig. 1). Each hybridized slide was insert into the fluorescence detector to capture the specimen shape (Fig. 1A) and fluorescent images of cy5 (MMP-2 and MMP-9) and cy3 (ECD; Fig. 1B). To determine the fluorescence intensities, 50-μm measuring circles were set (Fig. 1C, upper panel) to cover the whole specimen. In each circle, the fluorescence intensities of cy5 and cy3 were designated as the ratio of cy5 to cy3 (Fig. 1C, lower panel). We then selected the measuring circles covering normal glands, which are used as a built-in control for expressions of MMP-2, MMP-9, and ECD (Fig. 1D), to calculate the mean cy5-to-cy3 ratio. The cy5-to-cy3 ratios from measuring circles covering the tumor area were standardized to the mean cy5-to-cy3 ratio, which was set to 1.0, and was designated as MER. The MER was represented by a bar graph, to observe the value and distribution of MERT with the histological appearance (Fig. 1E). To evaluate for the mRNA integrity, we confirmed the gains in fluorescence intensities in each measuring circle. If the gain was lower than 200, we judged the mRNA integrity to be insufficient for assaying, and omitted the material.

2.5. Image analysis and the MER in CISH

The histologic image was captured by a photomicroscope (Carl Zeiss, Tokyo, Japan) equipped with 3CCD camera (Sony Corp., Tokyo, Japan). The images were analyzed by Optimas image analysis software (Optimas Corp., Bothell, WA). The detail of image analysis was described previously [4]. For CISH assay, 1 mm fields were examined along the whole length of the tissue core (Fig. 1) [5]. Gene expression was assessed in normal tissues (at least 2 fields for built-in control) for specimens. Within each field, at least 10 cells (range 10–20) with adequate cytoplasm permitting measurement of staining intensity were analyzed. Areas of nuclear staining and necrotic cells were avoided. Staining of the cells was next quantified to derive an average value of the field. All specimens used in the present study exhibited strong staining for the poly dT_{20} probe, indicating that the mRNA was well preserved. We adjusted specific gene expression by the poly dT_{20} in each slide in order to compare expression levels in different slides. This is analogous to a loading control used in mRNA Northern analysis. In addition, on each slide the gene expression levels in tumor epithelium were further normalized to the expression in histologically normal epithelium on the same slide to control for samples. The intensity of staining for each gene was evaluated by measuring the integrated O.D. of the poly $d(T)_{20}$ probe for each specimen as well as the specific mRNA probe of interest in both histologically normal and tumor epithelium. The O.D for a specific gene of interest was divided by the poly dT_{20} expression level in the same area to adjust for the mRNA integrity. The resulting normalized value obtained in tumor epithelium was divided by value obtained from measuring expression levels in non-tumorous epithelium. This ratio was multiplied via 100 and represented relative corrected gene expression in tumor vs. histologically normal epithelium. The MMP:E-cadherin ratio was calculated using the corrected mRNA expression levels in the following formula: (MMP-2 + MMP-9)/2 ÷ E-cadherin expression level.

2.6. Image analysis of VEGF-C

For the bicolor FISH assay, a fluorescence detector (Genetix, New Milton, UK) and microarray analysis software (QuantArray; GSI Lumonics Inc., Northville, MI) were used (Fig. 1). Each hybridized slide was inserted into the fluorescence detector (Genetix) to capture the specimen shape and fluorescent images of cy5. To determine the fluorescence intensities, 50-μm measuring circles were set as similar to MER analysis. In each circle, the fluorescence intensity of cy5 was measured. The cy5 intensities from measuring circles covering the tumor area were standardized to the mean cy5 intensity of normal glands, which was set to 100. The highest cy5 intensity was designated as VEGF-Cmax. The mean cy5 intensity of the specimen was designated as VEGF-Cmean.

2.7. Immunohistochemistry

Consecutive 4-μm sections were cut from each block. Immunohistochemistry was performed as described previously [21]. Briefly, an immunoperoxidase technique was applied following antigen retrieval with pepsin (DAKO

stage, (E) relation of the LVD to the VEGF-C_{max}, and (F) relation of the FISH-based MER to the VEGF-C_{max}, (G) relation of the FISH-based MER to the LVD, and (H) relation of the LVD with the pathologic stage. R = Spearman's rho.

tapraid2/zr5-uro/zr5-uro/zr599908/zr50690d08z | nairre | S=1 | 6/10/10 | 5:21 | Art: 6839 | ce: 19

Corp.) treatment for 20 min. After endogenous peroxidase block by 3% H_2O_2 and methanol for 15 minutes, the specimens were rinsed with PBS. Anti-D2-40 antibody (a marker for lymph duct endothelial cells recognizing sialoglycoprotein type O; Signet Laboratories Inc., Dedham, MA; diluted at 0.5%) was used as the primary antibody. After 2 hours incubation at room temperature, the specimens were again rinsed with PBS and treated for 1 hour at room temperature with the secondary antibody, peroxidase-conjugated anti-rabbit (Medical Biological Laboratories Co., Ltd., Nagoya, Japan; diluted at 0.5%). The specimens were then rinsed with PBS and color-developed with diaminobenzidine (DAB) solution (DAKO Corp.). After washing, the specimens were counterstained with Meyer's hematoxylin (Sigma Chemical Co., St. Louis, MO). Immunostaining of all samples was performed under the same conditions of antibody reaction and DAB exposure. The specimens immunostained with anti-D2-40 antibody were observed under 200× magnification and 5 areas with high D2-40 staining were picked up ("hot spot"). The areas with the maximum MER were also selected. These areas were captured by digital imaging with the CCD camera (Sony). The LVD was measured in the computer-captured image with NIH Image.

2.8. Statistical analyses

Statistical differences between two parameters (i.e., MER by bicolor FISH vs. MER by CISH, MER vs. Gleason score, MER vs. stage, VEGF-C vs. stage, and LVD vs. stage) were tested by the non-parametric Mann-Whitney *U* test. Correlation of the two parameters (i.e., VEGF-Cmax vs. VEGF-Cmean, and MER vs. LVD) was tested by the Spearman's rank correlation test. All statistical analyses were carried out with StatView ver. 4.5 (SAS Institute, Inc., Cary, NC), and a P value of less than 0.05 was considered statistically significant.

3. Results

3.1. Comparison of MER detected by the bicolor FISH with that by CISH

The MER was examined by computer-assisted bicolor FISH using 36 prostate cancer specimens (Fig. 1A–E). The same specimen was examined by the CISH to calculate MER (Fig. 1F). In the representative case, the highest MER detected by the bicolor FISH was 7.5 at the edge of the capsule side of the tumor. In contrast, the highest MER by the CISH was 8.8 at the same region where the highest MER was detected by bicolor FISH. MERs were examined by both the bicolor FISH and the CISH in 36 prostate cancer specimens. MER detected by bicolor FISH was compared with that detected by CISH (Fig. 1G). MERs detected by the two methods showed significant correlation (Spearman's r = 0.9056, $P < 0.0001$). From these finding, MER detected by bicolor FISH was thought to be reliable as that detected by CISH.

3.2. Comparison between MER detected by the bicolor FISH and Gleason score or stage

We compared the MER with the Gleason score (Fig. 2A): the MER distinguished Gleason score 8–10 cancers from Gleason score 7 cancers ($P < 0.0001$) and Gleason score 6 cancers from Gleason score 7 cancers ($P = 0.0159$). We then compared the MER with the pathologic stage (Fig. 2B): the MER also distinguished metastatic cancers (pT3a-b/N1) from extra-organ extended cancers (pT3a-b/N0; $P = 0.0016$) and organ-confined cancers (pT2) from extra-organ extended cancers (pT3a-b/N0; $P < 0.0001$).

3.3. Comparison between MER detected by the bicolor FISH and lymphangiogenesis

The MER was associated with lymph nodes metastasis. We then examined mRNA expression of VEGF-C (Fig. 3A and B) by 2 methods: expression in the field where the maximum MER was detected (VEGF-C_{max}) and expression in the whole tumor area (VEGF-C_{mean}). Both the expressions were standardized to those in the normal glands. The VEGF-C_{max} was well correlated with the VEGF-C_{mean} (Fig. 2C, $P < 0.0001$). The VEGF-C_{max} distinguished metastatic cancers from extra-organ extended cancers ($P = 0.0046$) and organ-confined cancers from extra-organ extended cancers ($P < 0.0001$).

Finally, we examined the LVD by anti-D2-40 immunostaining at the 5 hot spots and the area with maximum MER (Fig. 3C and D). As shown in Fig. 2E, LVD values were correlated with the VEGF-C_{max} (Spearman's r = 0.5908, $P < 0.0001$). The VEGF-C_{max} was concordant with the area with maximum MER in 63 (94%) of the 67 cases. VEGF-C_{max} was correlated with MER (Fig. 2F, Spearman's r = 0.8491, $P < 0.0001$). Moreover, LVD was correlated with MER (Fig. 2G, Spearman's r = 0.5569, $P < 0.0001$). The LVD also distinguished metastatic cancers from extra-organ extended cancers (Fig. 2H, $P < 0.0001$).

4. Discussion

The MER is a good marker for disease progression and/or prognosis of prostate, pancreatic, colon, gastric, and lung cancers {Anzai, 1996 #5; Herbst, 2000 #397}; [4,5,20,22]. The colorimetric MER distinguishes organ-confined tumors (pT2) from extra-organ extended tumors (pT3a-b/N0), as reported previously [4,5]. In our prospective study, the MER detected in prostatic core needle biopsy specimens was correlated with the final pathologic staging in 34 (87%) of 39 cases [23]. In 5 other cases where there was a failure to distinguish pT2 from pT3a-b/N1, the misdiagnosis was significantly associated with a small number of biopsies,

tapraid2/zr5-uro/zr5-uro/zr599908/zr50690d08z | nairre | S=1 | 6/10/10 | 5:21 | Art: 6839 | ce: 19

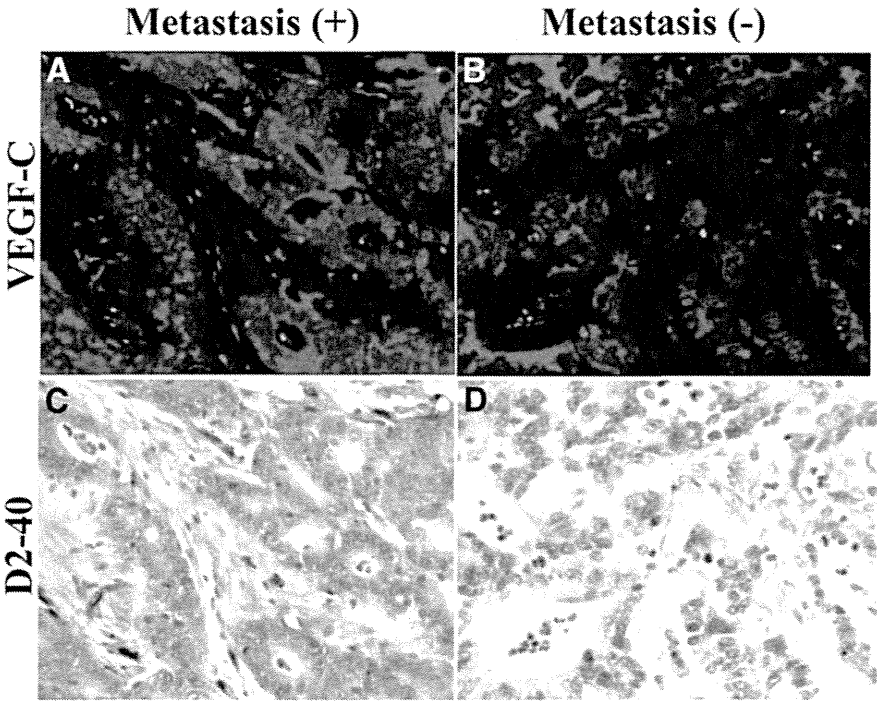

Fig. 3. VEGF-C expression and LVD of prostate cancer. (A) and (B) FISH assay of VEGF-C and (C) and (D) immunohistochemistry of lymph vessel by anti-D2-40 antibody in a metastatic prostate cancer case [(A) and (C); pT3aN1] and a nonmetastatic cancer case [(B) and (D); pT3aN0]. Scale bar = 50 μm.

small amount of tumor tissue in the biopsy specimens, and high intratumoral heterogeneity. In the present study, we selected cases tat contained adequate cancer contents (more than 2 mm in total specimens) to ensure the comparison between the bicolor FISH-based MER and CISH-based MER by avoiding statistical errors enlarged by sampling problems. This selection might result in an overabundance of pT3 disease concomitantly. In these cases, 4 of 26 T3a-b/N0 cases failed to be distinguished from T2 cases by CISH-based MER. In contrast, FISH-based MER completely distinguished T3a-b/N0 cases from T2 cases. Thus, FISH-based MER showed higher accuracy than CISH-based MER.

Another problem with the CISH-based MER is an observer-based error. To detect the highest MER, observers examine 20 points in each prostatectomy specimen or 1 point in every 1-mm length of core biopsy specimen [4,5]. In these methods, the number of measuring points is sufficient but does not encompass the whole specimen. For improving the observer-to-observer variation in the method, well-trained pathologists are needed to select the measuring points. To avoid these problems, in the present study, we investigated a new method to estimate the MER by using a bicolor FISH technique and detection system equipped with a computerized fluorescence detector, which is prepared for DNA array analyses.

The computer-assisted MER does not measure absolute expression levels of mRNA but the relative expression level of MMP-2 or MMP-9 to ECD in a single thin-section specimen. This method provides advantages to adjust mRNA retaining among the specimens or measuring points. Cancer tissues were distinguished from noncancerous tissues by H and E staining of the specimen used for ISH. Poly$(dT)_{20}$ analysis was substituted by evaluation of the signal gain in FISH. The new method is expected to enable easier application of the MER to clinical trials. The method can scan whole sample areas of prostatic core needle biopsy specimens by semiautomatic setting of the measuring circles, which can diminish the observation deviation or sampling error. The expression levels of MMP-2, MMP-9, and ECD were determined for each specimen, which can avoid slide-to-slide error.

We already examined the expression of VEGF in prostatic core needle biopsy tissues [4]. VEGF expression is well associated with the pathologic stage of the cases as well as the MER; however, the distributions of high VEGF expression values are different from those of the MER. The MER is higher at the periphery of the tumors, in contrast to VEGF expression, which is higher within the tumors [4,5]. In the present study, we examined VEGF-C mRNA expression by FISH and compared it with the MER. High values of both expressions were well correlated. In 63 (94%) of the 67 cases, the $VEGF_{max}$ was found at the same measuring point in the specimens.

VEGF-C expression is well correlated with MMP-2 expression in ovarian cancer [24]. Patients with lymph node metastasis

tapraid2/zr5-uro/zr5-uro/zr599908/zr50690d08z | nairre | S=1 | 6/10/10 | 5:21 | Art: 6839 | ce: 19

have higher serum VEGF-C and plasma MMP-9 concentrations than those without metastasis [25]. Coexpression of VEGF-C and MMP-2 is closely associated with lymph node metastasis in papillary thyroid cancer [26]. Expressions of VEGF-C and MMPs are up-regulated by the same upstream factors, such as RalA [27,28]. The VEGF-C intracellular signal activates the Prox1 transcription factor, inducing MMP-2 expression and extracellular matrix turnover [29,30]. Our results showing that the MER is correlated with VEGF-C expression might be a result of these molecular associations.

In conclusion, the dual-fluorescent computer-assisted MER using prostate core needle biopsy specimens might be a good marker for predicting the final pathologic stage with an easier technique and less human deviations than the CISH assay.

Uncited references

This section consists of references that are included in the reference list but are not cited in the article text. Please either cite each of these references in the text or, alternatively, delete it from the reference list. If you do not provide further instruction for these references, we will retain them in their current form and publish them as an "uncited reference" with your article: [31–36].

References

[1] D'Amico AV, Whittington R, Malkowicz SB, et al. The combination of preoperative prostate specific antigen and postoperative pathologic findings to predict outcome in clinically localized prostate cancer. J Urol 1998;160:2096–101.

[2] Kattan MW, Eastham JA, Stapleton AM, et al. A preoperative nomogram for disease recurrence following radical prostatectomy for prostate cancer. J Natl Cancer Inst 1998;90:766–71.

[3] Partin AW, Kattan MW, Subong ENP, et al. The use of prostate-specific antigen, clinical stage, and Gleason score to predict pathologic stage in men with localized prostate cancer: A multi-institutional update. J Am Med Assoc 1997;277:1445–51.

[4] Kuniyasu H, Troncoso P, Johnston D, et al. Relative expression of type IV collagenase, E-cadherin, and vascular endothelial growth factor/vascular permeability factor in prostatectomy specimens distinguishes organ-confined from pathologically advanced prostate cancers. Clin Cancer Res 2000;6:2295–308.

[5] Kuniyasu H, Ukai R, Johnston D, et al. The relative mRNA expression levels of matrix metalloproteinase to E-cadherin in prostate biopsy specimens distinguishe organ-confined from advanced prostate cancer at radical prostatectomy. Clin Cancer Res 2003;9:2185–94.

[6] Fidler IJ, Kripke ML. Genomic analysis of primary tumors does not address the prevalence of metastatic cells in the population. Nat Genet 2003;34:23.

[7] Fidler IJ. The pathogenesis of cancer metastasis: The 'seed and soil' hypothesis revisited. Nat Rev Cancer 2003;3:453–8.

[8] Das S, Skobe M. Lymphatic vessel activation in cancer. Ann NY Acad Sci 2008;1131:235–41.

[9] Arya M, Bott SR, Shergill IS, et al. The metastatic cascade in prostate cancer. Surg Oncol 2006;15:117–28.

[10] Ordon M, Nam RK. Lymph node assessment and lymphadenectomy in prostate cancer. J Surg Oncol 2009;99:215–24.

[11] Swanson GP, Thompson IM, Basler J. Current status of lymph node-positive prostate cancer: Incidence and predictors of outcome. Cancer 2006;107:439–50.

[12] Achen MG, Stacker SA. Molecular control of lymphatic metastasis. Ann NY Acad Sci 2008;1131:225–34.

[13] Lohela M, Saaristo A, Veikkola T, et al. Lymphangiogenic growth factors, receptors, and therapies. Thromb Haemost 2003;90:167–84.

[14] Wissmann C, Detmar M. Pathways targeting tumor lymphangiogenesis. Clin Cancer Res 2006;12:6865–8.

[15] Sasahira T, Kirita T, Oue N, et al. High mobility group box-1-inducible melanoma inhibitory activity is associated with nodal metastasis and lymphangiogenesis in oral squamous cell carcinoma. Cancer Sci 2008;99:1806–12.

[16] Tille JC, Nisato R, Pepper MS. Lymphangiogenesis and tumor metastasis. Novartis Foundation Symp 2004;256:112–31.

[17] Greene FL, Page DL, Fleming ID, et al. AJCC Cancer Staging Manual. New York: Springer-Verlag, 2003.

[18] Radinsky R, Bucana CD, Ellis LM, et al.. A rapid colorimetric in situ messenger RNA hybridization technique for analysis of epidermal growth factor receptor in paraffin-embedded surgical specimens of human colon carcinomas. Cancer Res 1993;53:937–43.

[19] Bucana CD, Radinsky R, Dong Z, et al. A rapid colorimetric in situ mRNA hybridization technique using hyperbiotinylated oligonucleotide probes for analysis of *mdr*-1 in mouse colon carcinoma cells. J Histochem Cytochem 1993;41:499–506.

[20] Kuniyasu H, Ellis LM, Evans DB, et al. Relative expression of E-cadherin and type IV collagenase genes predicts disease outcome in patients with resectable pancreatic carcinoma. Clin Cancer Res 1999; 5:25–33.

[21] Kuniyasu H, Oue N, Wakikawa A, et al. Expression of receptors for advanced glycation end-products (RAGE) is closely associated with the invasive and metastatic activity of gastric cancer. J Pathol 2002; 196:163–70.

[22] Kitadai Y, Ellis LM, Tucker SL, et al.. Multiparametric in situ mRNA hybridization analysis to predict disease recurrence in patients with colon carcinoma. Am J Pathol 1996;149:1541–51.

[23] Ohmori H, Fujii K, Sasahira T, et al. Determinants for prediction of malignant potential by metalloproteinase:E-cadherin ratio in prostate core needle biopsy. Pathobiology 2006;73:98–104.

[24] Ueda M, Hung YC, Terai Y, et al. Vascular endothelial growth factor-C expression and invasive phenotype in ovarian carcinomas. Clin Cancer Res 2005;11:3225–32.

[25] Tamura M, Oda M, Matsumoto I, et al. The combination assay with circulating vascular endothelial growth factor (VEGF)-C, matrix metalloproteinase-9, and VEGF for diagnosing lymph node metastasis in patients with non-small cell lung cancer. Ann Surg Oncol 2004;11:928–33.

[26] Tian X, Cong M, Zhou W, et al. Relationship between protein expression of VEGF-C, MMP-2, and lymph node metastasis in papillary thyroid cancer. J Int Med Res 2008;36:699–703.

[27] Aguirre-Ghiso JA, Frankel P, Farias EF, et al. RalA requirement for v-Src- and v-Ras-induced tumorigenicity and overproduction of urokinase-type plasminogen activator: involvement of metalloproteases. Oncogene 1999;18:4718–25.

[28] Rinaldo F, Li J, Wang E, et al. RalA regulates vascular endothelial growth factor-C (VEGF-C) synthesis in prostate cancer cells during androgen ablation. Oncogene 2007;26:1731–8.

[29] Papoutsi M, Dudas J, Becker J, et al. Gene regulation by homeobox transcription factor Prox1 in murine hepatoblasts. Cell Tissue Res 2007;330:209–20.

[30] Tammela T, Petrova TV, Alitalo K. Molecular lymphangiogenesis: New players. *Trends Cell Biol 2005;15*:434–41. AQ: 4

[31] Kuniyasu H, Oue N, Sasahira T, et al. Reg IV enhances peritoneal metastasis in gastric carcinomas. Cell Prolif 2009;42:110–21.

[32] Mitani Y, Oue N, Matsumura S, et al. Reg IV is a serum biomarker for gastric cancer patients and predicts response to 5-fluorouracil-based chemotherapy. Oncogene 2007;26:4383–93.

tapraid2/zr5-uro/zr5-uro/zr599908/zr50690d08z | nairre | S=1 | 6/10/10 | 5:21 | Art: 6839 | ce: 19

[33] Oue N, Kuniyasu H, Noguchi T, et al. Serum concentration of Reg IV in patients with colorectal cancer: overexpression and high Reg IV serum level is associated with liver metastasis. Oncology 2008;72:371–80.

[34] Bishnupuri KS, Luo Q, Korzenik JR, et al. Dysregulation of Reg gene expression occurs early in gastrointestinal tumorigenesis and regulates anti-apoptotic genes. Cancer Biol Ther 2006;5:1714–20.

[35] Bishnupuri KS, Luo Q, Murmu N, et al. Reg IV activates the epidermal growth factor receptor/Akt/AP-1 signaling pathway in colon adenocarcinomas. Gastroenterology 2006;130:137–49.

[36] Ohara S, Oue N, Matsubara A, et al. Reg IV is an independent prognostic factor for relapse in patients with clinically localized prostate cancer. Cancer Sci 2008;99:1570–7.

Diabetes-associated angiotensin activation enhances liver metastasis of colon cancer

Takasumi Shimomoto, Hitoshi Ohmori, Yi Luo, Yoshitomo Chihara, Ayumi Denda, Tomonori Sasahira, Naokuni Tatsumoto, Kiyomu Fujii & Hiroki

Clinical & Experimental Metastasis
Official Journal of the Metastasis Research Society

ISSN 0262-0898

Clin Exp Metastasis
DOI 10.1007/s10585-012-9480-6

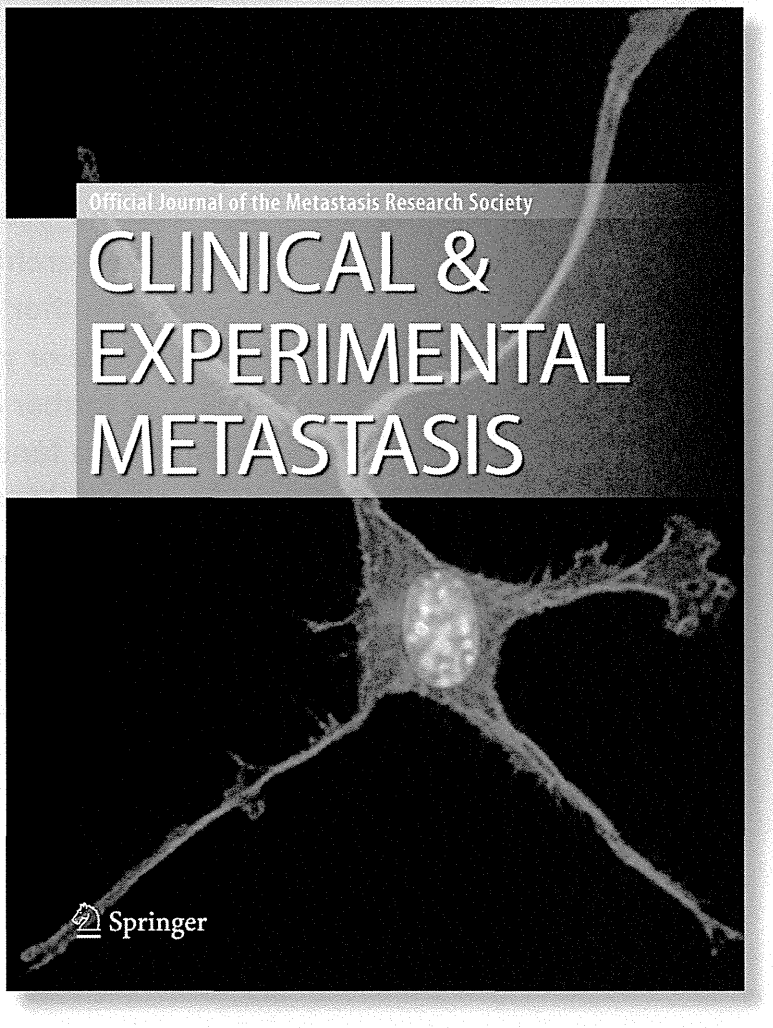

Springer

Clin Exp Metastasis
DOI 10.1007/s10585-012-9480-6

RESEARCH PAPER

Diabetes-associated angiotensin activation enhances liver metastasis of colon cancer

Takasumi Shimomoto · Hitoshi Ohmori · Yi Luo · Yoshitomo Chihara · Ayumi Denda · Tomonori Sasahira · Naokuni Tatsumoto · Kiyomu Fujii · Hiroki Kuniyasu

Received: 24 August 2011 / Accepted: 23 April 2012

Abstract We examined the effects of hyperglycemic conditions on liver metastasis of colorectal cancer (CRC). Angiotensin (A)-II increased growth, invasion, and anti-apoptotic survival in HT29 and CT26 cells. In contrast, angiotensinogen (ATG) increased these features in HT29 cells but not in CT26 cells. HT29 cells expressed A-II type 1 receptor, chymase, and rennin, whereas CT26 cells did not express renin. Renin expression and ATG-induced cell growth, invasion, and survival induced and increased as glucose concentration increased in HT29 cells and also CT26 cells. An inhibitor of renin or chymase abrogated A-II production in HT29 cells. Reduction of hepatic ATG production by cholesterol-conjugated antisense *S*-oligodeoxynucleotide suppressed liver metastasis of HT29 cells. An examination of 121 CRC patients showed that diabetes in CRC cases was associated with higher blood HbA1c, higher renin and A-II concentrations in the primary tumors, and higher incidence of liver metastasis than in nondiabetic cases. These results suggest that diabetes-associated angiotensin activation enhances liver metastasis of CRC and may therefore provide a possible target for antimetastatic therapy in CRC.

Keywords Angiotensin · Angiotensinogen · Renin · Chymase · Colorectal cancer · Liver metastasis

T. Shimomoto · H. Ohmori · Y. Luo · Y. Chihara · A. Denda · T. Sasahira · K. Fujii · H. Kuniyasu (✉)
Department of Molecular Pathology, Nara Medical University, 840 Shijo-cho, Kashihara, Nara 634-8521, Japan
e-mail: cooninh@zb4.so-net.ne.jp

N. Tatsumoto
Department of Surgery, Miyoshi Central Hospital, Miyoshi, Japan

Abbreviation

CRC	Colorectal cancer
ATG	Angiotensinogen
A-I	Angiotensin I
A-II	Angiotensin II
ATR-1	Angiotensin II type 1 receptor
ACE	Angiotensin converting enzyme
MAPK	Mitogen-activated protein kinase
ODN	Oligodeoxynucleotide
ARB	Angiotensin II type 1 receptor blocker

Introduction

Colorectal cancer (CRC) is the fourth leading cause of cancer death in Japan, and the cancer mortality is still increasing as the Western lifestyle gains popularity among the Japanese population [1]. Approximately 24 % of CRC cases involving invasion beyond the submucosal layer showed liver metastasis during and/or after the operation [2]. One-third of CRC patients died of liver metastasis [3]. Only one-third or fewer CRC patients with liver metastasis respond to systemic chemotherapy, however, and long-term survival is rare [3]. Early detection and control of liver metastasis is therefore an important issue for the treatment of CRCs.

Angiotensin-II (A-II) has multiple physiologic effects; activation of A-II type 1 receptor (ATR1) by A-II eventually leads to vasoconstriction, inflammation, and proliferation in cardiovascular and neoplastic tissues [4]. ATR1 intracellular signaling pathways produce diverse effects: ATR1 induces activation of protein kinase C, angiopoietin 2, vascular endothelial growth factor (VEGF), VEGF receptors, fibroblast growth factor, platelet-derived growth factor, transforming growth factor beta, epidermal growth

Published online: 03 May 2012